

Sequences of Einstein-Yang-Mills-Dilaton Black Holes

Burkhard Kleihaus, Jutta Kunz and Abha Sood
Fachbereich Physik, Universität Oldenburg, Postfach 2503
D-26111 Oldenburg, Germany

October 18, 2018

Abstract

Einstein-Yang-Mills-dilaton theory possesses sequences of neutral static spherically symmetric black hole solutions. The solutions depend on the dilaton coupling constant γ and on the horizon. The SU(2) solutions are labelled by the number of nodes n of the single gauge field function, whereas the SO(3) solutions are labelled by the nodes (n_1, n_2) of both gauge field functions. The SO(3) solutions form sequences characterized by the node structure $(j, j + n)$, where j is fixed. The sequences of magnetically neutral solutions tend to magnetically charged limiting solutions. For finite j the SO(3) sequences tend to magnetically charged Einstein-Yang-Mills-dilaton solutions with j nodes and charge $P = \sqrt{3}$. For $j = 0$ and $j \rightarrow \infty$ the SO(3) sequences tend to Einstein-Maxwell-dilaton solutions with magnetic charges $P = \sqrt{3}$ and $P = 2$, respectively. The latter also represent the scaled limiting solutions of the SU(2) sequence. The convergence of the global properties of the black hole solutions, such as mass, dilaton charge and Hawking temperature, is exponential. The degree of convergence of the matter and metric functions of the black hole solutions is related to the relative location of the horizon to the nodes of the corresponding regular solutions.

Preprint hep-th/9605109

1 Introduction

Motivated by higher-dimensional unified theories, such as Kaluza-Klein theory or superstring theory, where a scalar dilaton field arises naturally, static black hole solutions have been found in Einstein-Maxwell-dilaton (EMD) theory [1, 2]. In contrast to the static charged black holes of Einstein-Maxwell theory, referred to as Reissner-Nordström (RN) black holes, the charged EMD black holes exist for arbitrarily small event horizon, $x_H > 0$. The “extremal” solutions of EMD theory, obtained in the limit $x_H = 0$, possess a naked singularity at the origin.

Recently static black hole solutions have also been studied in Einstein-Yang-Mills-dilaton (EYMD) theory [3, 4, 5, 6, 7]. SU(2) EYMD theory possesses a sequence of magnetically neutral static spherically symmetric black hole solutions, labelled by the number of nodes n of the single gauge field function. The solutions exist for arbitrary event horizon $x_H > 0$ [3, 4, 5, 6, 7]. Here, in the limit $x_H \rightarrow 0$ regular particle-like solutions are obtained [3, 4, 5, 8, 6, 7].

For finite dilaton coupling constant γ , the sequence of regular neutral SU(2) EYMD solutions tends to the “extremal” EMD solution with the same dilaton coupling constant γ and with charge $P = 1$ for large n [4, 8]. For finite event horizon x_H and dilaton coupling constant γ , the corresponding sequence of neutral black hole solutions of SU(2) EYMD theory also tends to a limiting solution for large n . This limiting solution is the EMD black hole solution with the same event horizon x_H , the same dilaton coupling constant γ , and with magnetic charge $P = 1$ [7].

The magnetically neutral black hole solutions of EYMD theory have many features in common with those of Einstein-Yang-Mills (EYM) theory [9, 10, 11, 12]. In fact, in the limit of vanishing dilaton coupling constant γ , the EYMD black hole solutions approach those of EYM theory. In SU(2) EYM theory, the limiting solutions are the RN black holes with charge $P = 1$ and event horizon x_H , for $x_H > 1$ [13, 14, 15, 16]. For sequences of black holes with $x_H < 1$ and for the regular sequence [17], the limiting solutions are different [13, 14, 15, 16].

The non-abelian SU(2) black hole solutions do not possess a global YM charge. Since they are characterized not only by their mass but in addition by an interger n , they represent (unstable [18, 19, 20, 21, 22]) counterexamples to the “no-hair conjecture”. In contrast, SU(2) black holes with non-zero YM charge are uniquely characterized by their mass and charge. Indeed, for SU(2) all static spherically symmetric EYM black hole solutions with non-zero YM charge are embedded Reissner-Nordström solutions [23, 24]. This “non-abelian baldness theorem” no longer holds for SU(3), where black hole solutions with both Coulomb-like and essentially non-abelian gauge field configurations exist [25, 26]. While these black hole solutions [25, 26] correspond to SU(2)×U(1) solutions, the properties of genuine SU(3) black hole solutions have remained largely unknown.

The genuine magnetically neutral static spherically symmetric black hole solutions of SU(3) EYM and EYMD theory are based on the SO(3) embedding. These solutions can be labelled by the nodes (n_1, n_2) of both gauge field functions [27, 12, 7]. We have constructed SU(3) EYM and EYMD black hole solutions with a small number of nodes previously [12, 7], and we have identified two sequences of solutions together with their limiting solutions [7]. These sequences are the sequence $(0, n)$, containing the two lowest genuine SU(3) solutions, and the sequence (n, n) of scaled SU(2) solutions. The limiting solutions of these two sequences are again EMD solutions with the same event horizon and dilaton coupling constant, but with magnetic charges $P = \sqrt{3}$ and $P = 2$, respectively. The limiting solutions for $\gamma = 0$ and $x_H > P$ are the corresponding RN black holes.

For SU(3) EYMD theory it is not a priori clear, in which way the black hole solutions with general node structure (n_1, n_2) assemble to form sequences, converging to limiting solutions. One may expect though, that the limiting solutions of the general sequences of genuine SU(3) solutions are again magnetically charged solutions.

Here we construct genuine SU(3) black hole solutions with general node structure (n_1, n_2) . We show, that these solutions fall into sequences with node structure $(j, j+n)$, and we identify the limiting solutions of the new sequences with fixed finite j with the known magnetically charged SU(3) black hole solutions [26, 25]. We study the convergence of the matter and metric functions and of the global properties for these sequences of solutions.

In section 2 we derive the SU(3) EYMD equations of motion based on spherically symmetric ansätze for the metric and the matter fields. We discuss the boundary conditions and obtain relations between the metric and the dilaton field. In section 3 we consider SU(2) EYMD black hole solutions. We investigate their dependence on the parameters x_H and γ . We relate the degree of convergence of the matter and metric functions of the black hole solutions to the relative location of the horizon to the nodes of the corresponding regular solutions. We show, that the global properties of the solutions, such as mass, dilaton charge and Hawking temperature [28, 3, 5, 7], converge exponentially to those of the limiting solutions. In section 4 we discuss SU(3) EYMD black hole solutions. We identify the general set of sequences of genuine SU(3) solutions. We demonstrate that the convergence properties of these sequences are analogous to those of the SU(2) sequence. In section 5 we present our conclusions. In appendices A and B we review the limiting magnetically charged black hole solutions of EMD and EYMD theory. We demonstrate that the “extremal” EMD and EYMD solutions agree in many respects.

2 SU(3) Einstein-Yang-Mills-Dilaton Equations of Motion

2.1 SU(3) Einstein-Yang-Mills-Dilaton action

We consider the SU(3) Einstein-Yang-Mills-dilaton action

$$S = S_G + S_M = \int L_G \sqrt{-g} d^4x + \int L_M \sqrt{-g} d^4x \quad (1)$$

with

$$L_G = \frac{1}{16\pi G} R, \quad (2)$$

and matter Lagrangian

$$L_M = -\frac{1}{2} \partial_\mu \Phi \partial^\mu \Phi - e^{2\kappa\Phi} \frac{1}{2} \text{Tr}(F_{\mu\nu} F^{\mu\nu}), \quad (3)$$

where

$$F_{\mu\nu} = \partial_\mu A_\nu - \partial_\nu A_\mu - ig[A_\mu, A_\nu], \quad (4)$$

$$A_\mu = \frac{1}{2} \lambda^a A_\mu^a, \quad (5)$$

and g and κ are the gauge and dilaton coupling constants, respectively.

Variation of the action eq. (1) with respect to the metric $g^{\mu\nu}$ leads to the Einstein equations

$$G_{\mu\nu} = R_{\mu\nu} - \frac{1}{2} g_{\mu\nu} R = 8\pi G T_{\mu\nu} \quad (6)$$

with stress-energy tensor

$$\begin{aligned} T_{\mu\nu} &= g_{\mu\nu} L_M - 2 \frac{\partial L_M}{\partial g^{\mu\nu}} \\ &= \partial_\mu \Phi \partial_\nu \Phi - \frac{1}{2} g_{\mu\nu} \partial_\alpha \Phi \partial^\alpha \Phi + 2e^{2\kappa\Phi} \text{Tr}(F_{\mu\alpha} F_{\nu\beta} g^{\alpha\beta} - \frac{1}{4} g_{\mu\nu} F_{\alpha\beta} F^{\alpha\beta}), \end{aligned} \quad (7)$$

and variation with respect to the gauge field A_μ and the dilaton field Φ leads to the matter field equations.

2.2 Static spherically symmetric ansätze

To construct static spherically symmetric black hole solutions we employ Schwarzschild-like coordinates and adopt the spherically symmetric metric

$$ds^2 = g_{\mu\nu} dx^\mu dx^\nu = -A^2 N dt^2 + N^{-1} dr^2 + r^2 (d\theta^2 + \sin^2 \theta d\phi^2), \quad (8)$$

with

$$N = 1 - \frac{2m}{r} . \quad (9)$$

For SU(2) EYMD theory, the static spherically symmetric ansatz for the gauge field with vanishing time component is,

$$\begin{aligned} A_0 &= 0 , \\ A_i &= \frac{1 - w(r)}{2rg} (\vec{e}_r \times \vec{\tau})_i , \end{aligned} \quad (10)$$

with the SU(2) Pauli matrices $\vec{\tau} = (\tau_1, \tau_2, \tau_3)$. For SU(3) EYMD theory, generalized spherical symmetry for the gauge field is realized by embedding the SU(2) or the SO(3) generators in SU(3). In the SU(2)-embedding, the ansatz is given by (10) with $\vec{\tau}$ replaced by $\vec{\lambda} = (\lambda_1, \lambda_2, \lambda_3)$. In the SO(3)-embedding, the corresponding ansatz for the gauge field with vanishing time component is

$$\begin{aligned} A_0 &= 0 , \\ A_i &= \frac{2 - K(r)}{2rg} (\vec{e}_r \times \vec{\Lambda})_i + \frac{H(r)}{2rg} [(\vec{e}_r \times \vec{\Lambda})_i, \vec{e}_r \cdot \vec{\Lambda}]_+ , \end{aligned} \quad (11)$$

where $[,]_+$ denotes the anticommutator, and $\vec{\Lambda} = (\lambda_7, -\lambda_5, \lambda_2)$. For the dilaton field we take $\Phi = \Phi(r)$.

2.3 Field equations

For the above ansätze we now evaluate the tt and rr components of the Einstein equations. The metric (8) yields the components of the Einstein tensor

$$G_{tt} = \frac{2m'A^2N}{r^2} = 8\pi GT_{tt} = -8\pi GA^2NL_M , \quad (12)$$

and

$$G_{rr} = -\frac{G_{tt}}{A^2N^2} + \frac{2A'}{rA} = 8\pi GT_{rr} , \quad (13)$$

where the prime indicates the derivative with respect to r .

The spherically symmetric ansätze for the fields, eqs. (10) and (11), yield the tt and rr components of the stress-energy tensor, $T_{tt} = -A^2NL_M$, with

$$L_M = -\frac{1}{2}N\Phi'^2 - \frac{e^{2\kappa\Phi}}{g^2r^2} \left[Nw'^2 + \frac{1}{2r^2} (w^2 - 1)^2 \right] \quad (14)$$

and T_{rr}

$$T_{rr} = \frac{1}{N}L_M + \Phi'^2 + \frac{2e^{2\kappa\Phi}}{g^2r^2}w'^2 \quad (15)$$

for the SU(2) embedding, and with

$$L_M = -\frac{1}{2}N\Phi'^2 - \frac{e^{2\kappa\Phi}}{g^2r^2} \left[N(K'^2 + H'^2) + \frac{1}{8r^2} \left((K^2 + H^2 - 4)^2 + 12K^2H^2 \right) \right] \quad (16)$$

and

$$T_{rr} = \frac{1}{N}L_M + \Phi'^2 + \frac{2e^{2\kappa\Phi}}{g^2r^2}(K'^2 + H'^2) \quad (17)$$

for the SO(3) embedding.

Let us now introduce the dimensionless coordinate x ,

$$x = \frac{g}{\sqrt{4\pi G}}r, \quad (18)$$

(the prime indicating now the derivative with respect to x), the dimensionless mass function $\mu(x)$,

$$\mu = \frac{g}{\sqrt{4\pi G}}m = \frac{gm_{\text{Pl}}}{\sqrt{4\pi}}m, \quad (19)$$

the dimensionless dilaton field ϕ ,

$$\phi = \sqrt{4\pi G}\Phi, \quad (20)$$

and the dimensionless coupling constant γ ,

$$\gamma = \kappa/\sqrt{4\pi G}. \quad (21)$$

The choice $\gamma = 1$ corresponds to string theory, whereas $4 + n$ dimensional Kaluza-Klein theory has $\gamma^2 = (2 + n)/n$ [1].

With these definitions we then obtain the dimensionless EYMD equations. For SU(2) [3, 4, 5, 8, 6] the equations for the metric functions are

$$\mu' = \frac{1}{2}Nx^2\phi'^2 + e^{2\gamma\phi} \left[Nw'^2 + \frac{1}{2x^2} (w^2 - 1)^2 \right], \quad (22)$$

$$A' = \frac{2}{x} \left[\frac{1}{2}x^2\phi'^2 + e^{2\gamma\phi}w'^2 \right] A, \quad (23)$$

and the equations for the matter field functions are

$$(e^{2\gamma\phi}ANw')' = \frac{e^{2\gamma\phi}}{x^2}Aw(w^2 - 1), \quad (24)$$

$$(ANx^2\phi')' = 2\gamma Ae^{2\gamma\phi} \left[Nw'^2 + \frac{1}{2x^2} (w^2 - 1)^2 \right]. \quad (25)$$

For SO(3) [7], the equations for the metric functions are

$$\mu' = \frac{1}{2}Nx^2\phi'^2 + e^{2\gamma\phi} \left[N(K'^2 + H'^2) + \frac{1}{8x^2} \left((K^2 + H^2 - 4)^2 + 12K^2H^2 \right) \right] , \quad (26)$$

$$A' = \frac{2}{x} \left[\frac{1}{2}x^2\phi'^2 + e^{2\gamma\phi}(K'^2 + H'^2) \right] A , \quad (27)$$

and the equations for the matter field functions are

$$(e^{2\gamma\phi}ANK')' = \frac{e^{2\gamma\phi}}{4x^2}AK(K^2 + 7H^2 - 4) , \quad (28)$$

$$(e^{2\gamma\phi}ANH')' = \frac{e^{2\gamma\phi}}{4x^2}AH(H^2 + 7K^2 - 4) , \quad (29)$$

$$(ANx^2\phi')' = 2\gamma Ae^{2\gamma\phi} \left[N(K'^2 + H'^2) + \frac{1}{8x^2} \left((K^2 + H^2 - 4)^2 + 12K^2H^2 \right) \right] . \quad (30)$$

With help of eq. (23) for SU(2) or eq. (27) for SO(3) the metric function A can be eliminated from the matter field equations. Note that the SU(2) equations are symmetric with respect to the transformation $w(x) \rightarrow -w(x)$, and the SO(3) equations are symmetric with respect to both an interchange of the functions $K(x)$ and $H(x)$, and to the transformations $K(x) \rightarrow -K(x)$, and $H(x) \rightarrow -H(x)$, thereby yielding degenerate solutions.

2.4 Boundary conditions

Let us now consider the boundary conditions for the black hole solutions of EYMD theory. Requiring asymptotically flat solutions implies that the metric functions A and μ both must approach a constant at infinity. We here adopt

$$A(\infty) = 1 , \quad (31)$$

thus fixing the time coordinate. For magnetically neutral solutions the gauge field functions approach a vacuum configuration, i. e. for SU(2)

$$w(\infty) = \pm 1 , \quad (32)$$

and for SO(3)

$$K(\infty) = \pm 2 , \quad H(\infty) = 0 , \quad (33)$$

$$K(\infty) = 0 , \quad H(\infty) = \pm 2 . \quad (34)$$

For the dilaton field we choose [3, 4, 8, 6, 7, 29]

$$\phi(\infty) = 0 . \quad (35)$$

Magnetically charged solutions require different boundary conditions for the gauge field functions.

The existence of a regular event horizon at x_{H} requires for the metric functions

$$\mu(x_{\text{H}}) = \frac{x_{\text{H}}}{2} , \quad (36)$$

and $A(x_{\text{H}}) < \infty$. The matter functions must satisfy at the horizon x_{H}

$$N'w' = \frac{1}{x^2}w(w^2 - 1) , \quad (37)$$

$$N'\phi' = \frac{\gamma e^{2\gamma\phi}}{x^4}(w^2 - 1)^2 \quad (38)$$

for SU(2) and

$$N'K' = \frac{1}{4x^2}K(K^2 + 7H^2 - 4) , \quad (39)$$

$$N'H' = \frac{1}{4x^2}H(H^2 + 7K^2 - 4) , \quad (40)$$

$$N'\phi' = \frac{\gamma e^{2\gamma\phi}}{4x^4} \left[(K^2 + H^2 - 4)^2 + 12K^2H^2 \right] \quad (41)$$

for SO(3).

On considering the regular solutions, we observe that they satisfy the same boundary conditions at infinity as the black hole solutions. However, at the origin, regularity of the solutions requires

$$\mu(0) = 0 , \quad (42)$$

and the gauge field functions must satisfy

$$w(0) = \pm 1 , \quad (43)$$

for SU(2) and

$$K(0) = \pm 2 , \quad H(0) = 0 , \quad (44)$$

$$K(0) = 0 , \quad H(0) = \pm 2 , \quad (45)$$

for SO(3), and the dilaton field satisfies

$$\phi'(0) = 0 . \quad (46)$$

As in EYM theory [17, 12], it is sufficient to consider solutions with $w(0) = 1$ for SU(2) and with $K(0) = 2$ and $H(0) = 0$ for SO(3).

2.5 Relations between metric and dilaton field

Let us now derive relations between the dilaton field and the metric functions for purely magnetic (or electric) gauge fields of a general gauge group. For that purpose, we return to eq. (3) and introduce the gauge field Lagrangian L_A

$$L_M = -\frac{1}{2}\partial_\mu\Phi\partial^\mu\Phi + e^{2\kappa\Phi}L_A . \quad (47)$$

From the matter field action we then obtain the equation of motion for a static spherically symmetric dilaton field

$$(ANr^2\Phi')' = -2\kappa Ae^{2\kappa\Phi}r^2L_A , \quad (48)$$

where for the moment we retain the dimensioned quantities. Next we return to the tt component of the Einstein equations, eq. (12),

$$m' = 4\pi G \left(\frac{1}{2}Nr^2\Phi'^2 - \eta e^{2\kappa\Phi}r^2L_A \right) , \quad (49)$$

where $\eta = 1$ ($\eta = -1$) for purely magnetic (electric) gauge fields. With the help of this equation (49), we eliminate the gauge field from the dilaton equation (48)

$$(ANr^2\Phi')' = 2\eta\kappa A \left(\frac{m'}{4\pi G} - \frac{1}{2}Nr^2\Phi'^2 \right) . \quad (50)$$

We then consider the contracted Einstein equations. For purely magnetic (or electric) gauge fields the contracted gauge field stress energy tensor vanishes, yielding for the curvature scalar

$$R = 8\pi GN\Phi'^2 . \quad (51)$$

Thus the r.h.s of the dilaton equation (50) can be expressed purely in terms of metric functions

$$(ANr^2\Phi')' = \eta \frac{2\kappa}{4\pi G} \left(Am' - \frac{1}{4}Ar^2R \right) . \quad (52)$$

With

$$Ar^2R = - \left[r^2(2A'N + AN') \right]' + 4Am' \quad (53)$$

we then obtain for the dilaton field the equation

$$(ANx^2\phi')' = \frac{\eta}{2}\gamma \left(x^2(2A'N + AN') \right)' , \quad (54)$$

where we have returned to dimensionless quantities. This equation can be integrated, yielding

$$\phi' = \frac{\eta}{2}\gamma \left(\ln(A^2N) \right)' + \frac{C}{ANx^2} , \quad (55)$$

where C is an integration constant. In the following we only consider purely magnetic gauge fields ($\eta = 1$).

We are now interested in global relations between the metric and the dilaton field, involving the mass $\mu(\infty)$ and the dilaton charge D , which we define via

$$\phi(x) \xrightarrow{x \rightarrow \infty} -\frac{D}{x}. \quad (56)$$

We further introduce the dimensionless Hawking temperature T for the metric (8) [28, 3, 5, 7]

$$T = T_S A(1 - 2\mu')|_{x_H} = T_S x_H A N'|_{x_H}, \quad (57)$$

where $T_S = (4\pi x_H)^{-1}$ is the Hawking temperature of the Schwarzschild black hole.

We now integrate eq. (54) from the horizon to infinity. The asymptotic behaviour of the dilaton field is given by eq. (56). The metric functions approach constants asymptotically, $A(\infty) = 1$ and $N(\infty) = 1$ (see sect. 2.4), while their derivatives tend to zero [3, 4, 8]

$$A'(x) \xrightarrow{x \rightarrow \infty} O\left(\frac{1}{x^3}\right), \quad N'(x) \xrightarrow{x \rightarrow \infty} \frac{2\mu(\infty)}{x^2} + O\left(\frac{1}{x^3}\right). \quad (58)$$

At the horizon, the metric function $N(x_H)$ vanishes, while $N'(x_H)$ is related to the Hawking temperature (57). These boundary conditions then yield for the black holes the relation [7, 30]

$$D = \gamma \left(\mu(\infty) - \frac{1}{2} x_H^2 A N'|_{x_H} \right) = \gamma \mu(\infty) \left(1 - \frac{\mu_S}{\mu(\infty)} \frac{T}{T_S} \right), \quad (59)$$

where $\mu_S = x_H/2$ is the mass of the Schwarzschild black hole. Relation (59) holds for static, spherically symmetric, magnetic gauge fields of general gauge groups (provided the metric functions have the proper asymptotic behaviour). Thus besides the magnetically neutral SU(2) and SO(3) black holes considered here, relation (59) also holds for the magnetically charged EMD black holes [1, 2] and the magnetically charged SU(3) EYMD black holes [26].

The integration constant C in relation (55) is given by

$$C = D - \gamma \mu(\infty). \quad (60)$$

According to (59) it does not vanish for black holes in general [31]. Integration of eq. (55) therefore does not yield a simple expression for black holes.

Let us now consider the above relations for the regular solutions. By integrating eq. (54) from zero to infinity we obtain the simple relation [32]

$$D = \gamma \mu(\infty). \quad (61)$$

Consequently the integration constant C in eq. (55) vanishes for regular solutions. Integrating eq. (55) from x to infinity therefore gives the simple relation [32, 31]

$$\phi(x) = \frac{1}{2}\gamma \ln(A^2 N) = \frac{1}{2}\gamma \ln(-g_{tt}) . \quad (62)$$

Again, these relations are valid for static, spherically symmetric, magnetic gauge fields of general gauge groups.

3 SU(2) Einstein-Yang-Mills-Dilaton Black Holes

SU(2) EYMD theory possesses a sequence of magnetically neutral static spherically symmetric black hole solutions, which can be labelled by the number of nodes n of the gauge field function, $w_n(x)$ [3, 4, 5, 6, 7]. These black hole solutions exist for arbitrary dilaton coupling γ and for arbitrary event horizon $x_H > 0$. In the limit $x_H \rightarrow 0$, regular particle-like solutions are obtained [3, 4, 5, 8, 6, 7].

The sequences of SU(2) EYMD solutions converge to limiting solutions. In the following, we demonstrate numerically that in the limit $n \rightarrow \infty$, given a dilaton coupling constant γ and an event horizon x_H , the corresponding sequence of neutral SU(2) EYMD black hole solutions tends to the charged EMD black hole solution with the same dilaton coupling constant γ , the same event horizon x_H and with magnetic charge $P = 1$ [7]. This generalizes the earlier observation [4, 8], that for a given coupling constant γ , the sequence of regular neutral SU(2) EYMD solutions converges to the charged “extremal” EMD solution with the same coupling constant γ and with magnetic charge $P = 1$. (For completeness we review the EMD black hole solutions in appendix A.)

3.1 $\gamma = 1$

Since the coupling constant $\gamma = 1$ corresponds to the case of the low energy effective action of string theory, it deserves special attention. SU(2) black hole solutions for $\gamma = 1$ have been studied in [3, 6], where in [6] the effect of a small dilaton mass has additionally been considered.

We first discuss the properties of the black hole solutions of the stringy SU(2) sequence for a given event horizon. We relate the degree of convergence of the n -th EYMD solution with respect to the limiting EMD solution to the location of the event horizon. We observe, that the smaller the event horizon x_H , the larger is the value of the lowest n of the solution for which the functions have converged well.

Let us begin with a small event horizon $x_H = 0.01$. In Figs. 1a-e we present the lowest black hole solutions with an odd number of nodes, $n = 1, 3, 5$ and 7 for this event horizon. (Table 1 shows their dimensionless mass.) In particular, we present the

EYMD matter functions w_n and ϕ_n and metric functions N_n , A_n and P_n^2 , where the charge function P_n^2 is obtained from the metric coefficient g_{tt} according to [3]

$$g_{tt} = - \left(1 - \frac{2\mu(\infty)}{x} \sqrt{1 + \frac{D^2}{x^2} + \frac{P_n^2}{x^2}} \right), \quad (63)$$

such that $P = 1$ in the abelian limiting case. For comparison we also show the corresponding functions of the limiting EMD black hole solution, having the same horizon but magnetic charge $P = 1$.

Fig. 1a shows the EYMD gauge field functions w_n and the EMD function $w_\infty \equiv 0$. The value of w_n at the horizon decreases with increasing n towards the limiting value of zero. The location of the innermost node of w_n decreases with n , while the location of the outermost node of w_n increases with n , and thus w_n approaches the limiting value of zero in an increasingly larger region inbetween. The gauge field function w_7 is already close to zero over a region of many orders of magnitude. Obviously, with increasing n the EYMD gauge field functions w_n tend (nonuniformly) to the EMD function $w_\infty \equiv 0$.

As seen in Fig. 1b, with increasing n the EYMD dilaton functions ϕ_n also tend to the EMD function ϕ_∞ . The EYMD dilaton functions ϕ_n differ significantly from the EMD function ϕ_∞ only in an interior region, which decreases with n . Already for ϕ_7 there is no notable deviation from the limiting function to be observed.

Turning to the metric functions, we observe a similar pattern of convergence. As seen in Fig. 1c, the EYMD functions N_n tend to the EMD function N_∞ . The limiting EMD function N_∞ rises from zero at the event horizon to a plateau $N_\infty \approx 1/4$, and then rises further. Again, significant deviations between the EYMD and the EMD functions occur only in an interior region, which decreases with n . There the EYMD functions N_n develop a peak, decreasing in size with n . Again, for N_7 there is no notable deviation from the limiting function to be observed.

As seen in Fig. 1d, the EYMD metric functions A_n also tend to the EMD function A_∞ . Again, significant deviations between the EYMD and the EMD functions occur only in a decreasing interior region, and for A_7 there is no notable deviation from the limiting function to be observed.

In Fig. 1e the EYMD magnetic charge functions P_n^2 are seen and compared to the constant EMD magnetic charge, $P_\infty \equiv 1$. The magnetic charge P_n tends to the limiting value P_∞ in a large inner region, roughly limited by the outermost node of the EYMD gauge field function w_n . Beyond this region, the magnetic charge function decays rapidly to zero. (Only for $n = 1$ there is a significant deviation from the limiting magnetic charge even in the inner region.)

To understand this relation between the gauge field functions and the charge functions, we insert the asymptotic expansion (for large x) of the EYMD functions in

eq. (63). This yields for the magnetic charge function

$$P_n^2 = \frac{4}{3}\mu(\infty)D^2\frac{1}{x} + (w_{n(1)}^2 + \frac{2}{3}\mu^2(\infty)D^2)\frac{1}{x^2} + O(\frac{1}{x^3}) \quad (64)$$

where the constant $w_{n(1)}$ is the $(1/x)$ expansion coefficient of the gauge field function w_n , $w_n = (-1)^n + w_{n(1)}/x + O(1/x^2)$. The value of $w_{n(1)}$ is larger than $\mu(\infty)$ and D by six orders of magnitude, therefore the magnetic charge function has (up to a sign) approximately the same expansion coefficient as the gauge field function. The region where w_n reaches its asymptotic value is thus the same as the region where P_n decays to zero, i. e. the region beyond the outermost node of the gauge field function. Indeed, comparing the functions P_n^2 and $(w_n + 1)^2$, shown in Fig. 1e for $n = 7$, we observe, that they are very close beyond the outermost node of the gauge field function.

To gain more insight into the above observed pattern of convergence, let us consider for a moment the regular solutions. In Figs. 2a-b we show the regular EYMD gauge field functions w_n and metric functions N_n for $n = 1, 3, 5$ and 7 . The sequence of regular solutions converges to the “extremal” EMD solution [4, 8], which is also shown.

Let us now discuss some features of these solutions. With increasing n , the innermost node $z_n^{(1)}$ of the EYMD gauge field functions w_n decreases exponentially to zero, as seen in Fig. 2a (see also Table 2), whereas the outermost node increases exponentially. The boundary conditions for the gauge field functions w_n do not allow for a uniform convergence to the EMD function $w_\infty \equiv 0$. But the region where both EYMD and EMD functions are close increases exponentially with n . The EYMD metric functions N_n approach the value one at the origin, whereas the EMD function N_∞ monotonically approaches one quarter. Therefore there is again no uniform convergence of the EYMD functions to the limiting EMD function possible. But, as seen in Fig. 2b, the region, where the EYMD and EMD functions closely agree, again increases exponentially with n . We observe again that strong deviations of the functions N_n from the limiting function N_∞ occur only in an interior region, decreasing exponentially with n . In the vicinity of the innermost node $z_n^{(1)}$ of w_n , the function N_n has already come quite close to N_∞ , and beyond the second node $z_n^{(2)}$ of w_n both functions closely agree (with the exception of N_1).

The EYMD dilaton functions ϕ_n approach constant values close to the origin which decrease linearly with n . Further from the origin they approach the limiting EMD function ϕ_∞ . The interior regions, where the functions ϕ_n deviate significantly from the limiting solution ϕ_∞ , are limited by the respective location of the innermost node $z_n^{(1)}$ of w_n (with the exception of ϕ_1). The EYMD metric functions A_n exhibit an analogous pattern with respect to their convergence to the EMD function A_∞ . They deviate significantly from the limiting function in an interior region, extending slightly beyond the innermost node $z_n^{(1)}$ of w_n (with the exception of A_1).

Turning now back to the EYMD black hole solutions we observe, that the regular solutions have considerable influence on the black hole solutions for small horizon

size and that the innermost nodes of the regular EYMD gauge field functions largely determine the pattern of convergence. The location of these innermost nodes $z_n^{(1)}$ is presented in Table 2. In particular we note, that for the black hole solutions of Figs. 1, the location of the innermost node of the regular gauge field function with seven nodes is smaller than the event horizon $x_H = 0.01$. This fact has important consequences.

Considering the black hole gauge field functions w_n , we see that they are large at the horizon as long as the horizon is small compared to the location of the innermost node $z_n^{(1)}$ of the corresponding n -th regular gauge field function. Thus $w_1 - w_5$ are large at the horizon, whereas w_7 is small. Consequently, w_7 deviates strongly from the limiting function only in the far region where, beyond the last node, it must approach its boundary value. The black hole dilaton functions ϕ_n deviate significantly from the limiting function only in the interior region between the event horizon and the location of the innermost node $z_n^{(1)}$ of the corresponding n -th regular gauge field function. Thus there is no notable deviation left for ϕ_7 . The same is true for the metric functions N_7 and A_7 . Further, we now recognize that the peak in the functions $N_1 - N_5$, located shortly behind the event horizon, represents the tendency of these functions towards the corresponding regular metric functions. Also the functions N_n and A_n for $n < 7$ deviate significantly from the limiting functions only in the interior region between the event horizon and (slightly beyond) the location of the innermost node $z_n^{(1)}$ of the corresponding n -th regular gauge field function.

Choosing different values for the event horizon x_H we realize that the above observations are rather general. Considering solutions with event horizon $x_H = 0.1$, we see that already the location of the innermost node of the fourth regular gauge field function is smaller than x_H . Consequently, there are already for ϕ_4 , N_4 and A_4 no notable deviations from the limiting functions left. The convergence of the gauge field functions is somewhat slower, though w_5 is already small at the event horizon. Increasing the event horizon further to $x_H = 1$, shows that only the location of the innermost (and only) node of the first regular solution is still larger than the event horizon. Consequently, there are now already for ϕ_2 , N_2 and A_2 no notable deviations from the limiting functions left, while w_3 is small at the event horizon. For still larger horizons, $x_H \geq 10$, no notable deviations are left even for the functions ϕ_1 , N_1 and A_1 .

We demonstrate this dependence of the degree of convergence on the event horizon in Fig. 3, where we show the gauge field function w_7 for the event horizons $x_H = 0, 0.01, 0.1$ and 1 . A more quantitative analysis of the dependence of the degree of convergence of the functions is shown in Figs. 4a-b. There the functions Δw_n and $\Delta \phi_n$, defined as the relative deviations of the EYMD functions $(1 - w_n)$ and ϕ_n from the EMD functions $(1 - w_\infty)$ and ϕ_∞ at the horizon

$$\Delta w_n(x_H) = \frac{|(1 - w_n(x_H)) - (1 - w_\infty(x_H))|}{(1 - w_\infty(x_H))} = |w_n(x_H) - w_\infty(x_H)|, \quad (65)$$

$$\Delta\phi_n(x_H) = \frac{|\phi_n(x_H) - \phi_\infty(x_H)|}{|\phi_\infty(x_H)|}, \quad (66)$$

are shown as functions of the horizon for $n = 1 - 5$. Also shown are the locations of the two innermost nodes $z_n^{(1)}$ and $z_n^{(2)}$ of the corresponding regular solutions.

In Fig. 4a we observe, that the function $\Delta w_n(x_H)$ crosses the line indicating the location of the innermost node of the n -th regular solution, $z_n^{(1)}$, at a value of 0.27, for large n . $\Delta w_n(x_H)$ crosses the line indicating the location of the innermost node of the $(n - 1)$ -th regular solution, $z_{n-1}^{(1)}$ (which is located approximately halfway between the innermost and the second node), at a value of 0.05. (It crosses the line indicating the location of the innermost node of the $(n + 1)$ -th regular solution, $z_{n+1}^{(1)}$ at 0.75 .) Considering the function $\Delta\phi_n$, shown in Fig. 4b, we see, that $\Delta\phi_n$ is much smaller than Δw_n . In particular, the function $\Delta\phi_n$ crosses the line indicating $z_n^{(1)}$ at a value of approximately 0.01 for the larger n . We observe, that for the larger n , the crossings lie again on straight lines, which however have a small positive slope. Concluding we observe, that the solutions are converged well to the limiting solution for $x_H \gg z_n^{(1)}$.

Let us now consider the global properties of the solutions, the mass, the dilaton charge and the Hawking temperature. We recall, that these global properties are not independent, but related by relation (59). The dimensionless mass μ , the dilaton charge D and the Hawking temperature T/T_S for the black hole solutions with $n = 1 - 7$ and event horizons $x_H = 0, 0.01, 0.1$ and 1 are given in Table 1.

To discuss the inverse Hawking temperature $\beta = T^{-1}$ of the black hole solutions as a function of their mass $\mu(\infty)$, we first recall the case of the limiting EMD solution, which is special for $\gamma = 1$. Here the inverse Hawking temperature is a straight line as a function of mass, $T^{-1} = 4\pi X_+ = 8\pi\mu(\infty)$ (see appendix A). Note, that this is the same relation as the one obtained for Schwarzschild black holes. However, the EMD curve does not extend to the origin, since the ‘‘extremal’’ EMD solution has a finite mass and a finite temperature. For $P = 1$ this lower limiting mass is $1/\sqrt{2}$. In Fig. 5 we show the inverse Hawking temperature as a function of the mass for the EYMD black holes with $n = 1 - 4$. As expected, the curves converge rapidly towards the limiting EMD curve, also shown.

Let us now consider the convergence of the global properties of the black hole solutions in more detail. The mass, the dilaton charge and the Hawking temperature converge exponentially to the corresponding properties of the limiting EMD solution. To demonstrate this, we define $\Delta\mu_n$ as the deviation of the mass of the n -th EYMD solution from the mass of the limiting EMD solution and make an exponential ansatz for the n -dependence

$$\Delta\mu_n = \mu_\infty(\infty) - \mu_n(\infty) = a_\mu e^{-\alpha_\mu n}. \quad (67)$$

We define ΔD_n and ΔT_n for the dilaton charge and the Hawking temperature analo-

gously,

$$\Delta D_n = D_\infty - D_n = a_D e^{-\alpha_D n} , \quad (68)$$

$$\Delta T_n = \frac{T_n}{T_S} - \frac{T_\infty}{T_S} = a_T e^{-\alpha_T n} . \quad (69)$$

The coefficients a and α still depend on the parameters, the horizon x_H and the dilaton coupling constant γ .

A logarithmic convergence then requires the function $\ln(\Delta\mu_n)$ to be a straight line as a function of n . This is indeed the case, as seen in Fig. 6, for the regular solutions and for the black hole solutions with $x_H \geq 1$. However for small x_H and small values of n , we observe deviations from straight lines. These deviations are again related to the relative location of the horizon to the innermost nodes $z_n^{(1)}$ of the regular solutions. When the location of the innermost node of the n -th regular solution becomes smaller than the horizon, the values of $\ln(\Delta\mu_n)$ for the solutions with larger n fall on a straight line, whereas those for smaller n are close to the straight line of the regular solutions.

We observe, that the straight lines for the various finite values of the horizon are parallel, indicating the same coefficient α for all x_H . (The coefficient α is different for the regular solutions.) For small horizons the lines are roughly equally spaced; the same is true for large horizons. This suggests one to parametrize the coefficients α and a with the following x_H dependence

$$\alpha(x_H) = \text{const.} , \quad a(x_H) = \frac{b}{(x_H)^\delta} . \quad (70)$$

Approximately, we find $\alpha_\mu = 3.6$, $b_\mu = 1.2$ and $\delta_\mu = 2$ for small values of the horizon, $x_H \leq 1$, and the same α_μ but $b_\mu = 0.8$ and $\delta_\mu = 1$ for large values of the horizon, $x_H \gg 1$.

The functions $\ln(\Delta D_n)$ and $\ln(\Delta T_n)$ follow a similar pattern as the function $\ln(\Delta\mu_n)$. The coefficient α is approximately the same for all three functions, as expected, because of relation (59). Also the coefficients b and δ for the three functions are related, satisfying relation (59). In particular, $\delta_T = \delta_\mu + 1$. The constants α , b and δ for the mass, the dilaton charge and the Hawking temperature obtained by a mean square fit to our numerical data are given in Table 3.

In fact for large x_H one obtains an analytic handle on some of the coefficients. For instance, it follows analytically, that

$$\delta_\mu = \delta_D = 1 , \quad \delta_T = 2 , \quad (71)$$

and, allowing for general γ , one finds

$$b_D = 2\gamma b_\mu , \quad b_T = 2b_\mu , \quad (72)$$

which is indeed confirmed by the calculations.

3.2 $\gamma \neq 1$

In the following we discuss the convergence of the sequences of EYMD black hole solutions to the corresponding limiting EMD solutions for $\gamma \neq 1$. Note, that the values of γ in 4 + n -dimensional Kaluza-Klein theory, $\gamma^2 = (2 + n)/n$ [1] (with $n = 1, 2$ and 4 for U(1), SU(2) and SU(3), respectively), are in the range $\gamma > 1$. The limit $\gamma \rightarrow 0$ needs special consideration.

The EYMD black hole solutions and their limiting EMD solutions depend smoothly on the dilaton coupling constant for finite γ . Not surprisingly therefore, they follow the same pattern of convergence for any finite γ as for $\gamma = 1$. However, the degree of convergence of an EYMD black hole solution now also depends on γ . To analyze this dependence, let us inspect Table 2, where the location of the innermost node $z_n^{(1)}$ of the seven lowest regular EYMD gauge field functions is presented for the dilaton coupling constants $\gamma = 0.1, 0.5, 1$ and 2. For finite γ , the sequences of nodes $z_n^{(1)}$ approach zero exponentially with increasing n ,

$$z_n^{(1)}(\gamma) = d_\gamma e^{-c_\gamma n} . \quad (73)$$

The coefficients d_γ and c_γ increase with γ . Thus the nodes $z_n^{(1)}(\gamma)$ converge faster to zero for $\gamma > 1$ and slower for $\gamma < 1$, as compared to $\gamma = 1$.

The implications for the convergence of the sequences of EYMD black hole solutions are obvious. Let n be the number of nodes of the first EYMD black hole solution of a sequence with fixed horizon x_H , for which the functions have largely assumed their limiting values. Then n becomes smaller, the larger the value of the dilaton coupling constant γ . This is demonstrated in Figs. 7a-b, where we show the EYMD gauge field function w_γ and the metric function N_γ of the black hole solutions with dilaton coupling constants $\gamma = 0, 0.5, 1$ and 2 and event horizon $x_H = 0.01$, as well as the corresponding EMD solutions [33]. According to Table 2, the location of the innermost node $z_\gamma^{(1)}(\gamma)$ of the regular EYMD gauge field functions is larger than this horizon for $\gamma = 0$ and 0.5, so the corresponding EYMD black hole functions show large deviations from the limiting EMD functions in the inner regions. In contrast, for $\gamma = 1$ and 2, where $z_\gamma^{(1)}(\gamma) < x_H$, the EYMD functions have largely assumed their limiting EMD values.

The value $\gamma = 0$ is special, since EYMD theory then reduces to EYM theory. The limiting behaviour of the sequences of EYM black hole solutions with horizon x_H has been discussed before [13, 14, 15, 16]. For $x_H > 1$ the limiting solutions are the RN black hole solutions with charge $P = 1$. For black hole solutions with smaller event horizons and for the regular solutions the limiting solutions are more complicated, having a mass $\mu(\infty) = 1$, independent of the horizon [13, 14, 15, 16]. In this case the solutions must be considered separately in two regions, the inner region $x < 1$ and the outer region $x > 1$. In the outer region the limiting solution is given by the extremal RN black hole solution, while in the inner region the solution is of an oscillating type with $w_\infty \neq 0$ [13, 14, 15, 16].

Because of this different limiting behaviour of the black hole solutions for $\gamma = 0$ (and $x_H < 1$) the limit $\gamma \rightarrow 0$ is non-trivial. We will consider this limit separately elsewhere [34].

Let us now consider the inverse Hawking temperature β for general γ beginning with the limiting EMD black hole solutions. For $\gamma > 1$, the temperature in the “extremal” limit diverges, i. e. β is zero. The curve β versus mass then rises monotonically and approaches the Schwarzschild curve from below for large values of the horizon. For $0 < \gamma < 1$ the temperature in the “extremal” limit is zero, i. e. β diverges in the “extremal” limit. The curve β versus mass then falls to a minimum and approaches the Schwarzschild curve from above for large values of the horizon. For $\gamma = 0$ the Reissner-Nordström case is obtained. In contrast to the “extremal” EMD solutions, the extremal RN solution has a finite horizon, $x_H = \mu = P = 1$.

In Fig. 8, we show the convergence of the inverse temperature versus mass curves for the sequences of EYMD black holes with $n = 1 - 4$ to the corresponding curves for the limiting EMD black hole solutions for $\gamma = 0.5$ and 2. (The EYM case $\gamma = 0$ is shown in Fig. 5). Depending on the dilaton coupling constant γ and the number of nodes n , phase transitions can occur [5, 35, 7]. We observe, that for $\gamma \geq 1$ no phase transitions occur, since the inverse temperature curves rise monotonically for all n like the corresponding limiting EMD curves. In contrast, for $\gamma < 1$, phase transitions do occur for all members of a sequence beyond some critical $n_{\text{cr}}(\gamma)$. The reason for this behaviour is, that for $\gamma < 1$ the inverse temperature curve of the black hole solutions of a sequence approaches the inverse temperature curve of the corresponding limiting EMD black hole solutions from below. But while there is one phase transition along the limiting EMD curve, which starts from $\beta = \infty$, there are two phase transitions along the EYMD curves (beyond some critical n_{cr}), which start from $\beta = 0$ and therefore develop two extrema; a maximum and a minimum. The value $\gamma = 1$ is special in EYMD and EMD theory. Only for $\gamma < 1$ phase transitions can occur.

4 SU(3) Einstein-Yang-Mills-Dilaton Black Holes

Let us now turn to the magnetically neutral static spherically symmetric black hole solutions of SU(3) EYMD theory. Besides the solutions discussed in section 3, corresponding to the SU(2) embedding, SU(3) EYMD theory possesses magnetically neutral static spherically symmetric black hole solutions, corresponding to the SO(3) embedding. As in EYM theory [27, 12], these SO(3) solutions can be labelled by the nodes of both gauge field functions [7]. Here we adopt the classification of the solutions with respect to the node structure of the functions (u_1, u_2) [27, 12, 7],

$$u_1(x) = \frac{K(x) + H(x)}{2}, \quad u_2(x) = \frac{K(x) - H(x)}{2}. \quad (74)$$

We denote the number of nodes of the functions u_1 and u_2 by n_1 and n_2 , respectively, and the total number of nodes by n_T . (For $\text{SO}(3)$ solutions $n_T = n_1 + n_2$.) Due to the symmetry $H(x) \rightarrow -H(x)$ (see section 2.3), solutions with node structures (n_1, n_2) and (n_2, n_1) are equivalent, and it is sufficient to consider solutions with $n_1 \leq n_2$.

Previously, we have only constructed magnetically neutral $\text{SU}(3)$ EYMD and EYM black hole solutions with a small number of nodes [7, 12]. The lowest $\text{SO}(3)$ black hole solution has $n_T = 1$ and node structure $(0, 1)$, the second solution has $n_T = 2$ and node structure $(0, 2)$. The third and fourth solution have also $n_T = 2$, but both have the same node structure $(1, 1)$. Therefore the node structure (n_1, n_2) does not seem to classify the $\text{SO}(3)$ solutions uniquely. However, the third solution is a scaled $\text{SU}(2)$ solution, where $u_1 = u_2 = w$, and only the fourth solution is a genuine $\text{SO}(3)$ solution, where the two gauge field functions are not proportional. The two next solutions have $n_T = 3$ and node structure $(0, 3)$ and $(1, 2)$, respectively. We have listed the lowest solutions with $n_T \leq 5$ in Table 4, where their mass is shown for $\gamma = 1$ and several values of the horizon, $x_H = 0, 0.5, 1, 2$.

In our previous analysis [12, 7], we have identified two sequences of solutions: the genuine $\text{SO}(3)$ sequence $(0, n)$, containing the lowest $\text{SO}(3)$ solution, and the sequence (n, n) of scaled $\text{SU}(2)$ solutions. As in the $\text{SU}(2)$ case, the limiting solutions of these two neutral sequences are magnetically charged EMD solutions, with the same event horizon and the same dilaton coupling constant. However, their magnetic charges are $P = \sqrt{3}$ and $P = 2$, respectively [7]. We discuss the convergence of these sequences in detail below.

From our previous analysis [7, 12] it has not been clear yet, in which way $\text{SO}(3)$ black hole solutions with general node structure (n_1, n_2) assemble to form sequences, which converge to limiting solutions. Below we construct sequences from the neutral $\text{SU}(3)$ black hole solutions with general node structure (n_1, n_2) , and we identify the limiting solutions of these neutral sequences with the known magnetically charged $\text{SU}(3)$ black hole solutions [26, 25].

4.1 (n, n) sequences

The solutions with node structure (n, n) often come in pairs (see Table 4). One solution of the pair (n, n) exists always, this is the scaled $\text{SU}(2)$ solution. The second solution of the pair with node structure (n, n) is a genuine $\text{SO}(3)$ solution, whose existence depends on the parameters γ and x_H .

4.1.1 Scaled $\text{SU}(2)$ solutions

Comparison of the equations of motion of the $\text{SO}(3)$ embedding and those of the $\text{SU}(2)$ embedding shows, that to each $\text{SU}(2)$ solution there corresponds a “scaled $\text{SU}(2)$ ”

solution of the SO(3) system with precisely double the mass of its SU(2) counterpart. Introducing

$$x = 2\tilde{x} , \quad (75)$$

$$\mu(x) = 2\tilde{\mu}(\tilde{x}) , \quad (76)$$

$$K(x) = 2w(\tilde{x}) , \quad H(x) = 0 , \quad (77)$$

and

$$\phi(x) = \tilde{\phi}(\tilde{x}) , \quad (78)$$

the functions $\tilde{\mu}$, w and $\tilde{\phi}$ satisfy the SU(2) equations with coordinate \tilde{x} . Obviously, these scaled SU(2) solutions, having node structure (n, n) , then converge to the corresponding EMD solutions with scaled magnetic charge $P = 2$. Thus these solutions and their properties are obtained by simply scaling the solutions of section 3.

4.1.2 Genuine SO(3) solutions

Although the two gauge field functions u_1 and u_2 of the genuine SO(3) solutions have the same node structure (n, n) as the scaled SU(2) solutions, they are not proportional to each other. We now discuss the dependence of the genuine SO(3) solutions on the dilaton coupling constant and on the horizon. The regular solutions exist for all values of the dilaton coupling constant and (supposedly) for all values of n . Considering the SO(3) solution with node structure (n, n) as a function of the horizon for a fixed dilaton coupling constant, we observe, that it merges into the corresponding ‘‘scaled SU(2)’’ solution at a critical value of the horizon $x_{\text{H}}^{\text{cr}}(\gamma)$. This critical behaviour was first observed for vanishing dilaton coupling [12]. In the parameter ranges where the genuine SO(3) solutions exist, they have a slightly higher energy than their ‘‘scaled SU(2)’’ counterparts.

In Fig. 9, we show as an example the matter functions H and K of the genuine SO(3) solution $(5, 5)$ for $\gamma = 1$ and several values of the horizon. At the critical value $x_{\text{H}}^{\text{cr}} = 0.03$ the solution becomes identical to the ‘‘scaled SU(2)’’ solution, i. e. the gauge field function H vanishes identically. In Fig. 10, we show the critical value of the horizon x_{H}^{cr} as a function of the dilaton coupling constant γ for the lowest odd solutions, $n = 1, 3$ and 5 . The critical horizon first decreases as a function of the dilaton coupling constant, reaches a minimum and then increases linearly with γ , $x_{\text{H}}^{\text{cr}} = b(n)\gamma$ (with $b(1) = 0.677$, $b(3) = 0.0151$, $b(5) = 0.0004$) for $\gamma \gg 1$. Only for $\gamma = 0$ the critical value of the horizon $x_{\text{H}}^{\text{cr}}(n)$ converges with increasing n to a finite limit, $x_{\text{H}}^{\text{cr}}(\infty) = 1.3122$.

We further show in Fig. 10, the innermost nodes of the corresponding regular genuine SO(3) solutions as a function of the dilaton coupling constant. We observe, that for each value of n , the two curves closely follow each other. In general, the critical value of the horizon is slightly smaller than the innermost node of the corresponding regular SO(3) solution. Only for $n = 1$ the two curves cross at $\gamma = 0.9576$. (The curves

with the innermost nodes of the corresponding regular “scaled SU(2)” solutions also have the same shape but lie somewhat higher.) From our previous considerations on SU(2) black holes, this behaviour is not unexpected. There, when the horizon of the black hole becomes larger than the innermost node of the regular solution, the solution loses most of its structure. Here, since the genuine SO(3) black hole solutions have more structure than the “scaled SU(2)” black hole solutions, this additional structure disappears, and thus the genuine SO(3) solution disappears, when the horizon comes close to the vicinity of the innermost node of the regular SO(3) solution.

This observation demonstrates even more the importance of the innermost nodes of the regular solutions for the black hole solutions. For the SU(2) solutions, the innermost nodes of the regular solutions rule the pattern of convergence of the sequences of black hole solutions. For the genuine (n, n) SO(3) solutions, they determine the range of existence of the corresponding black hole solutions.

4.2 $(0, n)$ sequences

The two lowest neutral black hole solutions of the SO(3) embedding have node structure $(0, 1)$ and $(0, 2)$. They are the first members of the sequence $(0, n)$. For a given event horizon and dilaton coupling constant, this sequence tends to the EMD black hole solution with the same event horizon, the same dilaton coupling constant and with magnetic charge $P = \sqrt{3}$ [7]. Table 5 shows the dimensionless mass, the dilaton charge and the Hawking temperature for the lowest solutions of this sequence for $\gamma = 1$ and horizon $x_H = 1$.

Previously, we have only demonstrated the convergence of the global properties of this sequence. Here we consider in addition, the convergence of the spatial functions of the solutions of this sequence with increasing node number n . As in the SU(2) case, the location of the innermost node of the regular solution with n nodes determines the degree of convergence of the corresponding black hole solution with n nodes and horizon x_H . (Remember, that the nodes of the function $u_2(x)$ correspond to the intersections of the functions $K(x)$ and $H(x)$.) We observe that the black hole solution with n nodes has already largely converged to the corresponding limiting EMD solution, if the innermost node of the regular solution with n nodes is smaller than the horizon. It has not yet converged well, if the innermost node of the regular solution is larger than the horizon. Thus the pattern of convergence of the $(0, n)$ sequence is fully analogous to the SU(2) case. We demonstrate this in the following with a few examples.

Let us begin again with the case $\gamma = 1$, the case of the low energy effective action of string theory. In Figs. 11a-c, we show the matter functions K_n and H_n , and the metric functions N_n and P_n^2 for the small horizon $x_H = 0.2$ for $n = 1, 3$ and 5 . (The matter functions ϕ_n and the metric functions A_n are analogous to the SU(2) case and contain no relevant new information.) From Fig. 11a, we observe, that with increasing n , both

EYMD gauge field functions K_n and H_n approach the same limiting function

$$K_n(x) \xrightarrow{n \rightarrow \infty} \frac{f(x)}{\sqrt{2}}, \quad H_n(x) \xrightarrow{n \rightarrow \infty} \frac{f(x)}{\sqrt{2}}, \quad (79)$$

where f is constant

$$f(x) \equiv 1. \quad (80)$$

To relate this limiting function f to the corresponding EMD solution with charge $P = \sqrt{3}$ we inspect the EYMD equations of motion for the case $K = H = f/\sqrt{2}$. (These equations are presented in appendix B.) Indeed, for $f \equiv 1$ these equations reduce to the EMD equations of motion for a black hole with charge $P = \sqrt{3}$.

Let us now consider the degree of convergence of the black hole solutions of Figs. 11a-c with $x_H = 0.2$. For that purpose, we inspect the location of the innermost nodes of the gauge field functions of the corresponding regular solutions, which are given in Table 6. As for the regular SU(2) solutions, with increasing n the innermost nodes decrease exponentially to zero. For the example of Figs. 11a-c, the innermost nodes of the regular solutions are larger than the horizon for $n = 1$ and 3 and smaller than the horizon for $n = 5$. We conclude, that the solution with $n = 5$ should be close to the limiting EMD solution, also shown in Figs. 11a-c, whereas the solutions with $n = 3$ and $n = 1$ should still show large deviations from the limiting solution. This is indeed the case. The functions ϕ_5 , N_5 and A_5 are almost indiscernible from the limiting EMD functions, whereas the functions ϕ_3 , N_3 and A_3 deviate significantly from the limiting functions in the region interior to the innermost node. The gauge field functions K_n and H_n converge more slowly (and non-uniformly because of the boundary conditions at infinity), but $K_5 \approx H_5 \approx 1/\sqrt{2}$ already in a large region of space. Also the charge function P_5^2 has assumed its limiting value $P^2 = 3$ in a large region. In contrast, the charge function P_3^2 still deviates slightly from the limiting value in the inner region and P_1^2 deviates strongly.

We demonstrate the dependence of the black hole solutions on the horizon x_H in Fig. 12. There the gauge field functions K_5 and H_5 are shown for the event horizons $x_H = 0, 0.5, 1$ and 2. For the larger horizons, even the gauge field functions have converged well in the inner region. (For the regular solutions the boundary conditions inhibit a uniform convergence at the origin.) As for the SU(2) solutions, a more quantitative analysis of the degree of convergence of the solutions is obtained by studying the functions ΔK_n , ΔH_n and $\Delta \phi_n$, where the functions ΔK_n and ΔH_n , are defined as relative differences analogously to $\Delta \phi_n$ (eq. (66)). We observe, that the function $\Delta K_n(x_H)$ crosses the line indicating the location of the innermost node of the n -th regular solution, $z_n^{(1)}$, at the value 0.75 for the larger n , while the function $\Delta H_n(x_H)$ crosses at the value 0.60. Both functions have fallen to the value 0.05, when they cross the line indicating the location of the second node of the n -th regular solution, $z_n^{(2)}$. The

function $\Delta\phi_n$ is again much smaller than ΔK_n or ΔH_n and crosses the line indicating $z_n^{(1)}$ at a value on the order of 0.05 for the larger n .

The SO(3) solutions depend smoothly on the dilaton coupling constant γ . The γ dependence of the convergence properties of the sequences of black hole solutions is analogous to the SU(2) case. With increasing γ , the convergence of the sequences is faster, with decreasing γ the convergence is slower. This is seen from Table 6, where the innermost nodes of the lowest regular solutions of the $(0, n)$ sequence are given for $\gamma = 0.1, 0.5, 1$ and 2 .

Again, the limit $\gamma \rightarrow 0$ needs special consideration and will be discussed elsewhere [34]. However, we already note, that for $\gamma = 0$ the limiting solution is more complicated and analogous to the limiting SU(2) solution. For $x_H > P$ ($P = \sqrt{3}$), the limiting solution is the RN solution, while for $x_H < P$ the limiting solution is the extremal RN solution for $x > P$ and apparently an oscillating solution for $x < P$.

Let us now consider the convergence of the global properties of the solutions. Turning to the thermal properties of the black hole solutions first, we show in Fig. 13 the inverse Hawking temperature β as a function of the mass for the EYMD black holes for $n = 1 - 4$ and $\gamma = 1$ as well as $\gamma = 0$. As in the SU(2) case, the EYMD inverse temperature curves converge rapidly towards the limiting EMD and RN inverse temperature curves. Consequently, we also observe phase transitions, depending on the dilaton coupling constant and on the number of nodes. For instance, for $\gamma = 0$ and $n = 1$, there are two critical values of the mass, $\mu_1 = 1.561$ and $\mu_2 = 1.588$. The critical behaviour disappears beyond $\gamma = 0.0293$ for the lowest solution, while it occurs up to larger values of γ for the solutions with larger n . For $\gamma \geq 1$ no phase transitions occur.

The convergence of mass, dilaton charge and Hawking temperature is exponential, analogous to the SU(2) case. For the dilaton coupling constant $\gamma = 1$, these global properties are given in Table 5 for $n = 1 - 5$ together with their limiting values and the constants of the exponential approximation formulae eqs. (67)-(69) [36]. For large values of the horizon, the x_H -dependence in the approximation formulae can be extracted according to eq. (70). The corresponding parameters are shown in Table 7.

4.3 $(1, 1 + n)$ sequences

Let us now address the question, in which way the solutions with general node structure (n_1, n_2) assemble into sequences and to what limiting solutions these sequences converge. The existence of the sequence $(0, n)$, where one gauge field function has no node, whereas the other function has an increasing number of nodes, suggests one to examine the set of solutions, where one of the gauge field functions has one node, whereas the other function has an increasing number of nodes. We thus consider the set of solutions $(1, 1 + n)$. The first solution of this set is the solution $(1, 2)$; it has $n = 1$. (The solution $(1, 0)$ is equivalent to the solution $(0, 1)$ and belongs to the $(0, n)$ sequence. The

solutions $(1, 1)$ are members of the (n, n) sequences.) In the following, we demonstrate that for any value of the dilaton coupling constant γ and of the horizon x_H , the set of solutions $(1, 1 + n)$ indeed forms a sequence, tending to a limiting solution.

To identify the limiting solution, let us consider an example. In Figs. 14a-c we show the matter functions K_n and H_n , and the metric functions N_n and P_n^2 for the horizon $x_H = 0.2$ and $n = 1, 3$ and 5 for $\gamma = 1$. As for the $(0, n)$ sequence, in the limit $n \rightarrow \infty$ both EYMD gauge field functions K_n and H_n approach a single function $f(x)$. However, in contrast to the $(0, n)$ sequence, this function is not a constant; it depends on x and has one node. Obviously the limiting solution cannot be a magnetically charged EMD black hole. Instead the limiting solution turns out to be the lowest magnetically charged SU(3) black hole solution found in [26]. This limiting solution is also shown in Figs. 14a-c.

In fact, the simpler system of equations obtained with only one gauge field function, (see appendix B)

$$K(x) \equiv H(x) \equiv f(x)/\sqrt{2}, \quad (81)$$

possesses SU(3) black hole solutions with magnetic charge $P = \sqrt{3}$. Such charged black hole solutions have been constructed before for the dilaton coupling constants $\gamma = 1$ [26] and $\gamma = 0$ [25]. The equations for these charged black hole solutions closely resemble the SU(2) equations (and correspond to the SU(2) \times U(1) equations). Not surprisingly therefore, the charged black hole solutions form a sequence, which can be labelled by the number of nodes j of the single gauge field function f [26, 25]. Like the EMD black holes, for finite dilaton coupling constant γ , these charged black hole solutions with j nodes exist down to arbitrary small values of the horizon. In the “extremal” limit $x_H = 0$, the solutions present naked singularities like their EMD counterparts. (The “extremal” limit is discussed in appendix B.) In contrast, for vanishing coupling constant γ , the extremal black hole solutions have a finite horizon, $x_H = P$ ($P = \sqrt{3}$), analogous to the RN case [25].

Turning back to the $(1, 1 + n)$ sequence of EYMD solutions, we observe, that for any finite value of the dilaton coupling constant and any finite event horizon, the sequence of neutral black hole solutions tends to the magnetically charged SU(3) solution with one node, $j = 1$. This limiting solution has the same dilaton coupling constant, the same horizon, and it has magnetic charge $P = \sqrt{3}$. For finite dilaton coupling constant γ , the “extremal” solution with $j = 1$ represents the limiting solution of the regular neutral SO(3) sequence $(1, 1 + n)$. However, for zero coupling constant γ , the extremal black hole solution has a finite horizon, $x_H = P$, therefore the limiting solution is again more complicated for values of the horizon smaller than P [34].

The convergence properties of the solutions of the $(1, 1 + n)$ sequence are again analogous to those of the SO(3) $(0, n)$ sequence and the SU(2) sequence. The location of the horizon with respect to the innermost nodes of the function u_2 of the regular solutions determines the degree of convergence of the black hole solutions. The inner-

most nodes of the regular solutions are shown in Table 6 for several values of the dilaton coupling constant γ . For the example of Figs. 14a-c, the horizon is slightly smaller than the innermost node of the regular solution with $n = 3$. Consequently, the black hole solution with $n = 5$ has already converged well, the solution with $n = 3$ has almost converged, and the solution with $n = 1$ is far from convergence. Note the interesting shape of the limiting charge function $P_\infty^2(x)$, which is already approached well in the inner region by P_5^2 and in a smaller region by P_3^2 . The limiting charge function has two plateaus, an inner plateau at 3.790 and an outer plateau at the magnetic charge of the solution, $P^2 = 3$.

The global properties of the lowest solutions of the $(1, 1+n)$ sequence for $\gamma = 1$ and $x_H = 1$ are given in Table 5. The inverse temperature as a function of mass is shown for the lowest solutions of the $(1, 1+n)$ sequence and for the charged limiting $j = 1$ solution in Fig. 15 for $\gamma = 1$ and $\gamma = 0$. The exponential convergence of the global properties is demonstrated in Table 5 and Table 7 for $\gamma = 1$.

4.4 $(j, j + n)$ sequences

From the above results, it is clear, in which way the remaining $\text{SO}(3)$ solutions fall into sequences. The next sequence is formed by the solutions $(2, 2+n)$, beginning with the solution $(2, 3)$. In Figs. 16a-b, we show the matter functions K_n and H_n , and the charge functions P_n^2 for $n = 1, 3$ and 5 , the horizon $x_H = 0.2$, and the dilaton coupling constant $\gamma = 1$. In the limit $n \rightarrow \infty$, both EYMD gauge field functions K_n and H_n approach a single function $f(x)$ which has two nodes. This limiting function is the gauge field function of the magnetically charged $\text{SU}(3)$ EYMD black hole solution with two nodes, $j = 2$, and charge $P = \sqrt{3}$.

In general, we observe, that for any finite dilaton coupling constant γ , the $(2, 2+n)$ sequence of EYMD solutions tends to the corresponding magnetically charged $\text{SU}(3)$ solution with two nodes, $j = 2$, and magnetic charge $P = \sqrt{3}$. Considering the convergence properties of the solutions of the $(2, 2+n)$ sequence, we observe that they are again analogous to those of the above sequences $(0, n)$ and $(1, 1+n)$. The location of the horizon with respect to the innermost nodes of the regular solutions determines the degree of convergence of the black hole solutions.

In the example of Figs. 16a-b, the horizon is located well behind the innermost node of the regular solution with $n = 3$, as can be seen in Table 6 [38]. Consequently, the black hole solutions with $n = 5$ and $n = 3$ have already converged well, whereas the solution with $n = 1$ is still far from convergence. In particular, also the charge function P_∞^2 of the limiting solution is well approached in the inner region by P_5^2 and P_3^2 . We note, that the inner plateau of the limiting charge function has increased in height to 3.964 and has also increased in size. We further note, that the deviations ΔK_n fall on top of each other for $j = 0, 1$ and 2 , when regarded as functions of the scaled horizon

$x_{\text{H}}/z_5^{(1)}(j)$, and the same is true for the deviations ΔH_n .

The global properties of the lowest solutions of the $(2, 2+n)$ sequence are given in Table 5. The exponential convergence with n of the global properties is demonstrated in Tables 5 and 7, where we anticipate also an exponential convergence with j .

By generalizing the above observations we see, that (apart from the (n, n) solutions considered separately above) the neutral $\text{SO}(3)$ EYMD black hole solutions assemble into sequences $(j, j+n)$, with fixed index $j \geq 0$ and running index $n \geq 1$. For any finite value of the dilaton coupling constant and any finite event horizon, the sequence $(j, j+n)$ of neutral black hole solutions tends to the magnetically charged $\text{SU}(3)$ solution with j nodes, the same dilaton coupling constant, the same horizon, and with magnetic charge $P = \sqrt{3}$. For finite dilaton coupling constant γ , the ‘‘extremal’’ solution with j nodes represents the limiting solution of the regular neutral $\text{SO}(3)$ sequence $(j, j+n)$. (For coupling constant $\gamma = 0$, the limiting solution is the RN solution if $x_{\text{H}} > P$; it is again more complicated, if $x_{\text{H}} < P$ [34].)

Let us finally consider the sequence of the sequences $(j, j+n)$ of $\text{SO}(3)$ solutions, with running index j . The lowest $\text{SO}(3)$ sequence has $j = 0$. It approaches an EMD solution with magnetic charge $P = \sqrt{3}$ since $f \equiv 1$. The $(j, j+n)$ sequences approach the EYMD solutions with magnetic charge $P = \sqrt{3}$ and j nodes. In the limit $j \rightarrow \infty$, the limiting solutions of the sequences tend to a limiting solution themselves. This limiting solution has $f \equiv 0$, and therefore it is again an EMD solution. But this limiting EMD solution has magnetic charge $P = 2$. (It is also identical to the limiting solution of the sequence of scaled $\text{SU}(2)$ solutions.) The inverse temperature curves of the limiting charged solutions for $j = 1 - 4$ are shown in Fig. 17, together with the curves for $j = 0$ and $j = \infty$ for $\gamma = 1$ and $\gamma = 0$.

5 Conclusion

We have considered sequences of magnetically neutral, static, spherically symmetric black hole solutions of $\text{SU}(3)$ Einstein-Yang-Mills-dilaton theory, based on the $\text{SU}(2)$ embedding and on the $\text{SO}(3)$ embedding. Such sequences of black hole solutions exist for arbitrary dilaton coupling constant γ and arbitrary event horizon x_{H} . In the limit of vanishing event horizon, sequences of regular EYMD solutions are found. In the limit of vanishing dilaton coupling constant, sequences of EYM solutions are obtained.

The equations of motion for the EYMD system, together with the boundary conditions, allow for relations between the metric and the dilaton field. Black hole solutions satisfy a relation between mass and dilaton charge, $D = \gamma(\mu(\infty) - 2\pi x_{\text{H}}^2 T)$, where T is the Hawking temperature. Regular solutions satisfy two simple relations, $D = \gamma\mu(\infty)$ and $\phi(x) = \gamma \ln(\sqrt{-g_{tt}})$. These relations hold for static, spherically symmetric solutions with magnetic gauge fields of general gauge groups.

The members of the $\text{SU}(2)$ EYMD sequences are labelled by the number of nodes

n of the single gauge field function. In the limit of large n , for a given dilaton coupling constant γ and a given horizon x_H , the corresponding sequence of black hole solutions tends to the EMD black hole solution [1, 2] with magnetic charge $P = 1$, the same coupling constant and the same horizon. The corresponding sequence of regular EYMD solutions tends to the corresponding “extremal” EMD solution.

The solutions of the SO(3) embedding can be labelled by their node structure (n_1, n_2) , representing the number of nodes of both gauge field functions. The SO(3) solutions fall into sequences of two types. Most solutions belong to the first type, having node structure $(j, j + n)$, where j labels the sequence itself and n labels the members of the sequence, i. e. the lowest sequence has $j = 0$, the next $j = 1$, etc. The solutions of the second type have node structure (n, n) . Beside the “scaled SU(2)” solutions, there exist also genuine SO(3) solutions of this type. With regard to the genuine SO(3) solutions, the above labelling of the solutions by their node structure appears to be unique.

In the limit of large n , for a given dilaton coupling constant γ and a given horizon x_H , the corresponding sequence of black hole solutions with node structure $(j, j + n)$ and finite j tends to the magnetically charged SU(3) EYMD black hole solution with j nodes [26], which has the same coupling constant, the same horizon and magnetic charge $P = \sqrt{3}$. The corresponding sequences of regular solutions tend to the corresponding “extremal” magnetically charged EYMD solutions.

For $j = 0$ and $j \rightarrow \infty$, the magnetically charged EYMD SU(3) black hole solutions have constant gauge field functions. Therefore the limiting solutions in these cases are again charged EMD black hole solutions, having magnetic charges $P = \sqrt{3}$ and $P = 2$, respectively.

The genuine SO(3) solutions of type (n, n) differ from those of type $(j, j + n)$ in an important aspect. They do not exist for all values of the dilaton coupling constant γ and the horizon x_H . Instead, for each value of the coupling constant, there exists a critical value of the horizon, where the genuine SO(3) solution (n, n) merges into the corresponding “scaled SU(2)” solution.

In the case of vanishing dilaton coupling constant, the sequences of neutral EYM black hole solutions tend with increasing n to magnetically charged EYM black hole solutions [25] and to RN black hole solutions (for $(0, n)$ and scaled SU(2) (n, n)), as long as the horizon is larger than the magnetic charge. If the horizon is smaller than the magnetic charge, the limiting solutions are more complicated [13, 14, 15, 16, 34].

All sequences of black hole solutions exhibit the same pattern of convergence. The degree of convergence of a given EYMD black hole solution, labelled by n within the corresponding sequence, depends on the relative location of the horizon to the innermost node of the corresponding regular EYMD solution. If the horizon is larger than the location of this node, then the functions of the EYMD black hole solution have largely converged to the functions of the limiting solution. If the horizon is smaller than the

location of this innermost node, then the functions of the EYMD black hole solution still differ appreciably from those of the limiting solution, with a tendency to approach the functions of the regular EYMD solutions for small x .

The location of the innermost nodes of the regular EYMD solutions converges to zero exponentially, for all sequences. The larger (smaller) the dilaton coupling constant, the faster (slower) the convergence. For $\gamma = 0$ the location of the innermost nodes converges to a finite value for the various sequences.

For all sequences, the convergence of the global properties of the EYMD solutions, such as mass, dilaton charge and Hawking temperature, to those of the limiting charged solutions is exponential. The coefficients depend on the dilaton coupling constant γ , yielding a fast convergence for large γ and a slow convergence for small γ .

Obviously, the thermodynamic properties of the EYMD black hole solutions also tend to those of the corresponding limiting solutions for large n . The occurrence of phase transitions, where the specific heat changes sign, depends on the dilaton coupling constant γ . Only for $\gamma < 1$ phase transitions can occur.

Addressing the stability of the solutions, we note that the SU(2) and SU(3) EYM black hole solutions are unstable [18, 19, 21, 4, 22, 12], and so are the SU(2) EYMD black hole solutions [4]. We therefore conjecture, that the genuine SO(3) EYMD black hole solutions are also unstable. It appears to be interesting to study the number of unstable modes of the genuine SO(3) black hole solutions and look for a relation to the number of nodes of the solutions, in analogy to the SU(2) case, where the black hole solution with n nodes has $2n$ unstable modes [20, 21].

Acknowledgement

We dedicate this work to Larry Willets on the occasion of his retirement. We gratefully acknowledge discussions with M. Volkov.

6 Appendix A: Einstein-Maxwell-Dilaton Black Holes

We here briefly recall the well-known static, spherically symmetric EMD black hole solutions with magnetic charge P [1, 2]. Following the notation of [2], we introduce the coordinate X via

$$x = X \left(1 - \frac{X_-}{X} \right)^{\frac{\gamma^2}{1+\gamma^2}}, \quad (82)$$

$X = X_-$ then corresponds to the origin $x = 0$. (The coordinates x and X correspond to R and r of [2], respectively.) The metric then takes the form

$$ds^2 = -\lambda^2 dt^2 + \lambda^{-2} dX^2 + x^2 (d\theta^2 + \sin^2 \theta d\phi^2), \quad (83)$$

with

$$\lambda^2 = \left(1 - \frac{X_+}{X} \right) \left(1 - \frac{X_-}{X} \right)^{(1-\gamma^2)/(1+\gamma^2)}. \quad (84)$$

The non-vanishing component of the Maxwell field strength tensor is given by

$$F_{\theta\phi} = P \sin \theta \quad (85)$$

and the dilaton field by

$$e^{2\phi} = \left(1 - \frac{X_-}{X}\right)^{2\gamma/(1+\gamma^2)}. \quad (86)$$

The parameters X_+ and X_- are determined by the regular event horizon x_H

$$x_H = X_+ \left(1 - \frac{X_-}{X_+}\right)^{\frac{\gamma^2}{1+\gamma^2}} \quad (87)$$

and by the magnetic charge P

$$P = \left(\frac{X_+ X_-}{1 + \gamma^2}\right)^{\frac{1}{2}}. \quad (88)$$

The black hole solutions have mass $\mu(\infty)$

$$\mu(\infty) = \frac{X_+}{2} + \left(\frac{1 - \gamma^2}{1 + \gamma^2}\right) \frac{X_-}{2} \quad (89)$$

and dilaton charge D

$$D = \frac{\gamma X_-}{1 + \gamma^2}. \quad (90)$$

Thus they satisfy a quadratic relation between mass, dilaton charge and magnetic charge

$$\mu^2(\infty) + D^2 - P^2 = \left(\frac{X_+ - X_-}{2}\right)^2. \quad (91)$$

The EMD black hole solutions exist for arbitrary event horizon x_H . The limit $x_H \rightarrow 0$ is known as “extremal” limit. The “extremal” solutions have naked singularities at the origin. For finite horizon the solutions satisfy relation (59), whereas in the “extremal” limit they satisfy relations (61) and (62). For “extremal” EMD solutions the quadratic relation (91) between mass, dilaton charge and magnetic charge simplifies to

$$\mu = P/\sqrt{1 + \gamma^2}. \quad (92)$$

For comparison let us also note the metric functions A and N of the metric (8)

$$N = \frac{\lambda^2}{A^2}, \quad A = \frac{\partial X}{\partial x}. \quad (93)$$

For the “extremal” solutions

$$N(0) = \frac{\gamma^4}{(1 + \gamma^2)^2}. \quad (94)$$

6.1 $\gamma = 1$

For $\gamma = 1$ the above formulae simplify considerably. The relation between the coordinates x and X is easily inverted

$$X = \frac{X_- + \sqrt{X_-^2 + 4x^2}}{2} . \quad (95)$$

Eliminating the parameter X_- via

$$X_- = \frac{2P^2}{X_+} , \quad (96)$$

the parameter X_+ is determined by

$$X_+ = \sqrt{x_{\text{H}}^2 + 2P^2} \quad (97)$$

for a given horizon x_{H} and magnetic charge P . The mass, dilaton charge and Hawking temperature then are

$$\mu(\infty) = X_+/2 , \quad (98)$$

$$D = P^2/X_+ = \frac{P^2}{2\mu(\infty)} , \quad (99)$$

and

$$T/T_{\text{S}} = x_{\text{H}}/X_+ = \frac{x_{\text{H}}}{2\mu(\infty)} . \quad (100)$$

6.2 $\gamma = 0$

For $\gamma = 0$ the dilaton field decouples. The black hole solutions with magnetic charge P are simply the Reissner-Nordström solutions with metric (8), where

$$N = \left(1 - \frac{2\mu}{x} + \frac{P^2}{x^2} \right) , \quad A \equiv 1 . \quad (101)$$

The non-vanishing component of the Maxwell field strength tensor is given by eq. (85) as above. For magnetically neutral black holes the metric (101) reduces to the Schwarzschild metric, where $P = 0$.

7 Appendix B: Charged SU(3) Einstein-Yang-Mills Black Holes

A restricted subset of SU(3) EYMD black hole solutions with $K \equiv H$ has been studied previously [26]. These solutions correspond to magnetically charged black holes [26].

To derive their equations of motion, let us put $K = H = \frac{f}{\sqrt{2}}$ in the SO(3) equations, eqs. (26)-(30). This yields for the metric functions [39]

$$\mu' = \frac{1}{2}Nx^2\phi'^2 + e^{2\gamma\phi} \left[Nf'^2 + \frac{1}{2x^2} (f^2 - 1)^2 + \frac{3}{2x^2} \right] , \quad (102)$$

$$A' = \frac{2}{x} \left[\frac{1}{2}x^2\phi'^2 + e^{2\gamma\phi} f'^2 \right] A . \quad (103)$$

For the matter field functions we obtain the equations

$$(e^{2\gamma\phi} ANf')' = e^{2\gamma\phi} \frac{1}{x^2} Af (f^2 - 1) , \quad (104)$$

$$(ANx^2\phi')' = 2\gamma Ae^{2\gamma\phi} \left[Nf'^2 + \frac{1}{2x^2} (f^2 - 1)^2 + \frac{3}{2x^2} \right] . \quad (105)$$

These equations differ from the SU(2) equations only by the presence of the term $\frac{3}{2x^2}$ in the equations of μ and ϕ . In fact they correspond to magnetic SU(2) \times U(1) equations. In general a term of the form $\frac{P^2}{2x^2}$ is present for magnetically charged solutions with charge P . For the asymptotic behaviour of the gauge field function

$$f(x) \xrightarrow{x \rightarrow \infty} 1 , \quad (106)$$

the above solutions have magnetic charge $P = \sqrt{3}$, while for

$$f(x) \xrightarrow{x \rightarrow \infty} 0 , \quad (107)$$

their magnetic charge is $P = 2$.

Obviously, the condition $K \equiv H$ is in conflict with the boundary conditions (33) and (34), imposed on the gauge field functions of neutral black hole solutions at infinity. Neither can the boundary conditions (44) and (45), imposed for the gauge field function of regular solutions at the origin, be satisfied for solutions with $K \equiv H$. Therefore these solutions have no regular limit [25]. For $\gamma = 0$ there exists for any n an extremal black hole solution with finite horizon $x_H = P$, in close analogy to the extremal RN solution [25]. For $\gamma \neq 0$ the black hole solutions exist for any n down to arbitrary small horizon. In the limit $x_H \rightarrow 0$ an ‘‘extremal’’ solution is obtained [26].

In the following we show, that this ‘‘extremal’’ solution is closely analogous to the ‘‘extremal’’ EMD solution. To study the limit $x \rightarrow 0$, let us introduce new functions G and Γ [26] by

$$G = e^{\gamma\phi} , \quad \Gamma = \gamma x \phi' = \frac{xG'}{G} , \quad (108)$$

with

$$G \xrightarrow{x \rightarrow 0} G_0 x , \quad \Gamma \xrightarrow{x \rightarrow 0} 1 . \quad (109)$$

Inserting the small x expansion for the functions G and f in eqs. (102), (103) and (105), we obtain to lowest order

$$\mu' = \frac{1}{2} \frac{N}{\gamma^2} + \frac{1}{2} G_0^2 P^2, \quad (110)$$

$$\frac{x A'}{A} = \frac{1}{\gamma^2} \quad (111)$$

and

$$(ANx)' = \gamma^2 A G_0^2 P^2. \quad (112)$$

There are no contributions from the gauge field function to this order. Solving eqs. (110) and (111) gives to lowest order in x

$$\mu = \frac{1}{2} \frac{\gamma^2}{1 + \gamma^2} \left(\frac{1}{\gamma^2} + G_0^2 P^2 \right) x, \quad (113)$$

$$A = A_0 x^{\frac{1}{\gamma^2}}, \quad (114)$$

where A_0 is an integration constant. Eq. (112) then leads to

$$G_0^2 P^2 = \frac{1}{1 + \gamma^2}. \quad (115)$$

Thus we find to lowest order in x

$$\mu = \frac{1}{2} \frac{1 + 2\gamma^2}{(1 + \gamma^2)^2} x, \quad (116)$$

$$G = \frac{1}{\sqrt{P^2(1 + \gamma^2)}} x, \quad (117)$$

and at the origin

$$N(0) = \left(\frac{\gamma^2}{1 + \gamma^2} \right)^2. \quad (118)$$

To determine A_0 we note, that eq. (62) holds also for the “extremal” EYMD solutions. Rewriting eq. (62) in terms of $G(x)$ yields

$$G = (A^2 N)^{\gamma^2/2}. \quad (119)$$

Inserting the small x expansions, eqs. (114), (117) and (118), we find the constant A_0 ,

$$A_0 = \frac{1 + \gamma^2}{\gamma^2} \left(\sqrt{1 + \gamma^2 P} \right)^{-\frac{1}{\gamma^2}}. \quad (120)$$

G_0 , A_0 and $N(0)$ coincide with the corresponding expressions for the “extremal” EMD solutions in the limit $X_+ = X_-$.

Using the functions G and Γ instead of ϕ and ϕ' , we have constructed the “extremal” solutions numerically with the boundary conditions

$$G \xrightarrow{x \rightarrow \infty} 1, \quad \Gamma(0) = 1, \quad (121)$$

and the boundary conditions of the regular solutions for the other functions.

Let us finally calculate the inverse Hawking temperature of the “extremal” solutions. At the horizon the equations for μ and Γ are given by

$$\mu'_H = G_H^2 [\quad]_H, \quad \Gamma_H = \frac{2\gamma^2 G_H^2}{x_H N'_H} [\quad]_H. \quad (122)$$

(The index H indicates the value of the functions at the horizon, $[\quad]_H$ abbreviates an irrelevant expression.) Eliminating $G_H^2 [\quad]_H$ in eq. (122) we find

$$\mu'_H = \frac{\Gamma_H}{\Gamma_H + \gamma^2} \frac{\mu_H}{x_H}. \quad (123)$$

In the limit $x_H \rightarrow 0$ with $\Gamma_H \rightarrow 1$ and $\mu_H = \frac{x_H}{2}$ we obtain

$$\mu'_H \xrightarrow{x_H \rightarrow 0} \frac{1}{2} \frac{1}{1 + \gamma^2}, \quad \text{i.e.} \quad (xN')_H \xrightarrow{x_H \rightarrow 0} \frac{\gamma^2}{1 + \gamma^2}. \quad (124)$$

(Note, that the limit $x \rightarrow 0$ for the “extremal” solutions coincides with the limit $x_H \rightarrow 0$ of the black hole solutions for the functions G, Γ, A, f , but not for N .)

Using the small x behaviour of A , eqs. (114) and (120), the inverse Hawking temperature becomes in the limit of vanishing horizon

$$\beta(x_H) \xrightarrow{x_H \rightarrow 0} 4\pi \left(\sqrt{1 + \gamma^2 P} \right)^{\frac{1}{\gamma^2}} x_H^{\frac{\gamma^2 - 1}{\gamma^2}}. \quad (125)$$

Thus for the “extremal” EYMD solutions β is finite for $\gamma = 1$, it diverges for $\gamma < 1$ and vanishes for $\gamma > 1$, completely analogous to the inverse Hawking temperature of the “extremal” EMD solutions.

The limit of small horizon for the EYMD black hole solutions on the one hand and the limit of small x for the “extremal” EYMD solutions on the other hand coincide with the limiting behaviour of the corresponding EMD solutions. The reason is clearly, that there is no explicit contribution from the gauge field in this limit. Therefore, for $\gamma = 1$, β has the same value for the “extremal” EMD solution and for the “extremal” EYMD solutions with j nodes, as seen in Fig. 17.

References

- [1] G. W. Gibbons and K. Maeda, Black holes and membranes in higher-dimensional theories with dilaton fields, Nucl. Phys. B298 (1988) 741.
- [2] D. Garfinkle, G. T. Horowitz and A. Strominger, Charged black holes in string theory, Phys. Rev. D43 (1991) 3140.
- [3] E. E. Donets and D. V. Gal'tsov, Stringy sphalerons and non-abelian black holes, Phys. Lett. B302 (1993) 411.
- [4] G. Lavrelashvili and D. Maison, Regular and black hole solutions of Einstein-Yang-Mills dilaton theory, Nucl. Phys. B410 (1993) 407.
- [5] T. Torii and K. Maeda, Black holes with non-Abelian hair and their thermodynamical properties, Phys. Rev. D48 (1993) 1643.
- [6] C. M. O'Neill, Einstein-Yang-Mills theory with a massive dilaton and axion: String-inspired regular and black hole solutions, Phys. Rev. D50 (1994) 865.
- [7] B. Kleihaus, J. Kunz and A. Sood, SU(3) Einstein-Yang-Mills-dilaton sphalerons and black holes, Phys. Lett. B374 (1996) 289; preprint hep-th/9510069.
- [8] P. Bizon, Saddle points of stringy action, Acta Physica Polonica B24 (1993) 1209.
- [9] M. S. Volkov and D. V. Galt'sov, Black holes in Einstein-Yang-Mills theory, Sov. J. Nucl. Phys. 51 (1990) 747.
- [10] P. Bizon, Colored black holes, Phys. Rev. Lett. 64 (1990) 2844.
- [11] H. P. Künzle and A. K. M. Masoud-ul-Alam, Spherically symmetric static SU(2) Einstein-Yang-Mills fields, J. Math. Phys. 31 (1990) 928.
- [12] B. Kleihaus, J. Kunz and A. Sood, SU(3) Einstein-Yang-Mills sphalerons and black holes, Phys. Lett. B354 (1995) 240.
- [13] P. Breitenlohner, P. Forgacs and D. Maison, Static spherically symmetric solutions of the Einstein-Yang-Mills equations, Commun. Math. Phys. 163 (1994) 141.
- [14] J. A. Smoller and A. G. Wasserman, An investigation of the limiting behavior of particle-like solutions to the Einstein-Yang/Mills equations and a new black hole solution, Commun. Math. Phys. 161 (1994) 365.
- [15] P. Breitenlohner and D. Maison, On the limiting solution of the Bartnik-McKinnon family, Commun. Math. Phys. 171 (1995) 685.

- [16] J. A. Smoller and A. G. Wasserman, Limiting behavior of solutions to the Einstein-Yang/Mills equations, preprint gr-qc/9405003.
- [17] R. Bartnik and J. McKinnon, Particlelike solutions of the Einstein-Yang-Mills equations, *Phys. Rev. Lett.* 61 (1988) 141.
- [18] N. Straumann and Z. H. Zhou, Instability of colored black hole solutions, *Phys. Lett.* B243 (1990) 33.
- [19] M. S. Volkov and D. V. Gal'tsov, Odd-parity negative modes of Einstein-Yang-Mills black holes and sphalerons, *Phys. Lett.* B341 (1995) 279.
- [20] G. Lavrelashvili and D. Maison, A remark on the instability of the Bartnik-McKinnon solutions, *Phys. Lett.* B343 (1995) 214.
- [21] M. S. Volkov, O. Brodbeck, G. Lavrelashvili and N. Straumann, The number of sphaleron instabilities of the Bartnik-McKinnon solitons and nonabelian black holes, *Phys. Lett.* B349 (1995) 438.
- [22] O. Brodbeck and N. Straumann, Instability proof for Einstein-Yang-Mills solitons and black holes with arbitrary gauge groups, ZU-TH-38-94, gr-qc/9411058.
- [23] D. V. Gal'tsov and A. A. Ershov, Non-abelian baldness of colored black holes, *Phys. Lett.* A138 (1989) 160.
- [24] P. Bizon and O. T. Popp, No-hair theorem for spherical monopoles and dyons in SU(2) Einstein-Yang-Mills theory, *Class. Quantum Grav.* 9 (1992) 193.
- [25] D. V. Gal'tsov and M. S. Volkov, Charged non-abelian SU(3) Einstein-Yang-Mills black holes, *Phys. Lett.* B274 (1992) 173.
- [26] E. E. Donets and D. V. Gal'tsov, Charged stringy black holes with non-abelian hair, *Phys. Lett.* B312 (1993) 391.
- [27] H. P. Künzle, Analysis of the static spherically symmetric SU(n)-Einstein-Yang-Mills equations, *Comm. Math. Phys.* 162 (1994) 371.
- [28] I. Moss and A. Wray, Black holes and sphalerons, *Phys. Rev.* D46 (1992) R1215.
- [29] The equations of motion are invariant under a shift $\phi \rightarrow \phi + \phi_0$ together with a rescaling $x \rightarrow xe^{\gamma\phi_0}$. Therefore solutions regular at infinity can always be chosen to satisfy $\phi(\infty) = 0$ [3, 4].
- [30] An equivalent expression for SU(2) black holes for $\gamma = 1$ was obtained in [6].

- [31] An exception are the “extremal” magnetically charged EMD and EYMD solutions (see Appendices A and B).
- [32] The relations (61) and (62) generalize the relations obtained previously for SU(2) and $\gamma = 1$ [3, 8, 6, 26]. Ref. [8] contains a scaled version of relation (61) for SU(2) and general γ .
- [33] Relation (63) for P^2 can be generalized for $\gamma \neq 1$. In order to define the charge function for $\gamma \neq 0$, we start from $-x^2 g_{tt}^{(\text{EMD})} = (X - X_-)(X - X_+)$. We introduce the variable $\xi(X) = X - \gamma^2 \frac{P^2}{X_+} = X - \gamma D$, and employ $X_+ + X_- = 2(\mu(\infty) + \gamma D)$ and $X_- = \frac{1+\gamma^2}{\gamma} D$. We then find $-x^2 g_{tt}^{(\text{EMD})} = P^2 + \xi^2 - D^2 - 2\xi\mu(\infty)$, and we define the charge function $P(x)$ for the EYMD system by

$$P^2(x) = -x^2 g_{tt} - \xi^2(x) + 2\xi(x)\mu(\infty) + D^2 ,$$

with the function $\xi(x)$ implicitly given. With $y^2 = \xi^2 - D^2$ the equation for the charge function can be put into the form $-x^2 g_{tt} = P^2(y) + y^2 - 2\mu(\infty)\sqrt{y^2 + D^2}$, which coincides with (63) for $\gamma = 1$ (since $y^2 = x^2$).

- [34] B. Kleihaus, J. Kunz and A. Sood, in preparation.
- [35] The coupling of ref. [5] is related to ours via $\kappa = \sqrt{2}\gamma$.
- [36] The masses $\mu(\infty)$ of the regular solutions are well approximated by the formula $\mu(\infty, \gamma, n) = [\sqrt{3} - (\pi/2) \exp(-4n/3)]/(\sqrt{1 + \gamma^2})$ [7].
- [37] For $\gamma = 1$ and $x_H \leq 1$ many data points of the sequences $(0, n)$, $(1, 1 + n)$ and $(2, 2 + n)$ for $n \leq 5$ do not yet fall on straight parallel lines. This makes it difficult to extract the asymptotic behaviour for large n . Employing

$$\Delta\mu_{n,j}(\infty) = \mu_{\infty,j}(\infty) - \mu_{n,j}(\infty) = \frac{b_\mu}{x_H^2} e^{-(\alpha_\mu n + \bar{\alpha}_\mu j)} ,$$

(analogously for D) and

$$\Delta T_{n,j} = (T/T_s)_{n,j} - (T/T_s)_{\infty,j} = \frac{b_T}{x_H^3} e^{-(\alpha_T n + \bar{\alpha}_T j)} ,$$

we find for the coefficients $b_\mu \approx 6.7$, $b_D \approx 19.3$ and $b_T \approx 25.6$, and for the exponents $\alpha_\mu \approx \alpha_D \approx \alpha_T \approx 2.8$ and $\bar{\alpha}_\mu \approx \bar{\alpha}_D \approx \bar{\alpha}_T \approx 3.7$.

- [38] Table 6 shows, that the innermost nodes of the regular solutions decrease approximately exponentially with j for fixed n .
- [39] The equations of [26, 25] contain a scale factor R_e . They agree with our equations (102)-(105) for $R_e = 2$. The black hole solutions of [26] are presented for $R_e = 1$, and therefore tend to a scaled limiting solution with charge $P = 1$.

$\mu(\infty)$

n	x_H	.0	.01	.1	1.0
1		.57699	.57896	.59726	.83671
2		.68483	.68567	.69381	.86507
3		.70345	.70379	.70755	.86600
4		.70651	.70665	.70882	.86602
5		.70701	.70707	.70887	.86603
6		.70709	.70712	.70887	.86603
7		.70710	.70712	.70887	.86603

 D

n	x_H	.0	.01	.1	1.0
1		.57699	.57698	.57639	.51213
2		.68483	.68484	.68416	.57483
3		.70345	.70344	.70262	.57728
4		.70651	.70650	.70519	.57735
5		.70701	.70700	.70534	.57735
6		.70709	.70708	.70535	.57735
7		.70710	.70709	.70535	.57735

 T/T_S

n	x_H	.0	.01	.1	1.0
1		.39365	.39601	.41750	.64915
2		.16649	.16900	.19299	.58048
3		.06773	.07028	.09870	.57744
4		.02738	.03000	.07256	.57735
5		.01106	.01388	.07059	.57735
6		.00446	.00809	.07054	.57735
7		.00180	.00711	.07053	.57735

Table 1

The mass $\mu(\infty)$, dilaton charge D and Hawking temperature T/T_S for the SU(2) EYMD regular solutions ($x_H = 0$) and black hole solutions ($x_H = .01, .1$ and 1) with up to seven nodes n and dilaton coupling constant $\gamma = 1$.

n	γ			
	0.1	0.5	1.0	2.0
1	1.53846	1.42382	1.35402	1.62119
2	1.08289	.80649	.53637	.44233
3	.95933	.52922	.21751	.10992
4	.92289	.36395	.08791	.02606
5	.90328	.25272	.03550	.00612
6	.88668	.17577	.01434	.00143
7	.87082	.12229	.00579	.00034
c_γ	.018	.363	.907	1.451
d_γ	.988	1.550	3.308	8.661

Table 2

The location of the innermost node $z_n^{(1)}(\gamma)$ for the SU(2) EYMD regular solutions up to seven nodes n for several values of the dilaton coupling constant γ . The nodes are well approximated by $z_n^{(1)}(\gamma) = d_\gamma e^{-c_\gamma n}$, with constants d_γ , c_γ also shown.

	$0 < x_H \leq 1$			$10 \leq x_H < \infty$		
	$\mu(\infty)$	D	T/T_S	$\mu(\infty)$	D	T/T_S
δ	1.916	1.951	2.941	1.001	1.002	2.006
b	1.156	2.960	3.361	0.782	1.594	1.607
α	3.623	3.594	3.568	3.591	3.630	3.624

Table 3

The constants δ , b , α of the least square fits for $\Delta\mu_n = \mu_\infty(\infty) - \mu_n(\infty) = \frac{b_\mu}{(x_H)^{\delta_\mu}} e^{-\alpha_\mu n}$ (and analogous for D and T/T_S) for the SU(2) EYMD sequence for $\gamma = 1$. The fits have been done separately for the regions $0 < x_H \leq 1$ and $10 \leq x_H < \infty$.

$(j, j + n)$	x_H			
	0.	0.5	1.0	2.0
(0, 1)	.90853	1.02708	1.16497	1.49442
(0, 2)	1.14153	1.20944	1.30297	1.57396
(1, 1)*	1.15397	1.25989	1.38135	1.67341
(1, 1)	1.18797	1.27399	1.38437	—
(0, 3)	1.20383	1.24529	1.32140	1.58069
(0, 4)	1.21958	1.24966	1.32279	1.58111
(0, 5)	1.22347	1.24998	1.32287	1.58114
(1, 2)	1.32130	1.37840	1.46227	1.71399
(1, 3)	1.36195	1.39923	1.47209	1.71729
(2, 2)*	1.36967	1.42005	1.49382	1.73014
(1, 4)	1.37300	1.40151	1.47278	1.71750
(2, 2)	1.37417	—	—	—
(2, 3)	1.39866	1.43109	1.49813	1.73148

Table 4

The mass of the lowest regular ($x_H = 0$) and black hole ($x_H = 0.5, 1$ and 2) SO(3) EYMD solutions with a total number of nodes $n_T \leq 5$ and dilaton coupling constant $\gamma = 1$. The asterisk indicates the scaled SU(2) solutions. Note that the genuine SO(3) black hole solutions with node structure (n, n) do not exist for all horizons.

$(j, j + n)$	$\mu(\infty)$	D	T/T_S
(0, 1)	1.16497	.87027	.58942
(0, 2)	1.30297	1.08770	.43054
(0, 3)	1.32140	1.12979	.38322
(0, 4)	1.32279	1.13364	.37830
(0, 5)	1.32287	1.13388	.37798
(0, ∞)	1.32288	1.13389	.37796
α_μ^0	2.798	2.786	2.780
a_μ^0	6.529	17.582	22.235
(1, 2)	1.46227	1.26493	.39467
(1, 3)	1.47209	1.28839	.36740
(1, 4)	1.47278	1.29029	.36499
(1, 5)	1.47283	1.29041	.36484
(1, 6)	1.47283	1.29042	.36483
(1, ∞)	1.47283	1.29042	.36483
α_μ^1	2.773	2.748	2.727
a_μ^1	.180	.443	.527
(2, 3)	1.49813	1.32829	.33968
(2, 4)	1.49843	1.32917	.33853
(2, 5)	1.49845	1.32922	.33846
(2, 6)	1.49845	1.32922	.33845
(2, 7)	1.49845	1.32922	.33845
(2, ∞)	1.49845	1.32922	.33845
α_μ^2	2.806	2.801	2.803
a_μ^2	.005	.015	.020
(∞, ∞)	1.5	1.33333	.33333

Table 5

The mass $\mu(\infty)$, dilaton charge D and Hawking Temperatur T/T_S for the SO(3) EYMD black hole solutions of the sequences $(j, j + n)$ with $0 \leq j \leq 2$, $1 \leq n \leq 5$ for dilaton coupling constant $\gamma = 1$ and horizon $x_H = 1$. For each sequence the limiting values $\mu_\infty^j(\infty)$, D_∞^j and $(T/T_S)_\infty^j$ are given. The masses $\mu_n(\infty)$ are approximated by $\mu_\infty(\infty) - \mu_n(\infty) = a_\mu^j e^{-\alpha_\mu^j n}$ (and analogously D and T/T_S), with the constants a, α also shown. The last line contains the values obtained for $\mu_\infty^j(\infty)$, D_∞^j and $(T/T_S)_\infty^j$ in the limit $j \rightarrow \infty$.

	n	$j =$	0	1	2	c_n	d_n
$\gamma = 0.1$	1		2.47869	1.86167	1.69430	.094	2.046
	2		1.86074	1.64685	1.58248	.040	1.714
	3		1.64914	1.56969	1.53269	.024	1.608
	4		1.57468	1.53460	1.50527	.019	1.565
	5		1.53986	1.50966	1.48215	.018	1.538
	c_j		.034	.019	.017		
	d_j		1.821	1.663	1.611		
$\gamma = 0.5$	1		2.29374	1.34077	.89474	.404	2.009
	2		1.43827	.94746	.65374	.371	1.373
	3		1.01694	.69874	.48400	.367	1.009
	4		.75328	.52643	.36697	.361	.755
	5		.56598	.39571	.27491	.364	.570
	c_j		.293	.284	.283		
	d_j		2.443	1.640	1.133		
$\gamma = 1$	1		2.18639	.85307	.34698	.920	2.171
	2		1.02365	.42121	.17227	.891	1.025
	3		.50393	.20783	.08377	.897	.506
	4		.24955	.10352	.04215	.889	.250
	5		.12364	.05102	.02055	.897	.124
	c_j		.716	.704	.706		
	d_j		4.373	1.722	.704		
$\gamma = 2$	1		2.62983	.68046	.16794	1.376	2.651
	2		.91273	.23353	.05661	1.390	.921
	3		.31115	.07745	.01818	1.420	.314
	4		.10281	.02540	.00605	1.416	.103
	5		.03357	.00824	.00193	1.428	.034
	c_j		1.091	1.105	1.117		
	d_j		8.001	2.096	.520		

Table 6

The location of the innermost node $z_n^{(1)}$ for the SO(3) EYMD regular solutions with node structure $(j, j+n)$ with $j \leq 2$ and $n \leq 5$ for the dilaton coupling constants $\gamma = 0.1, 0.5, 1, 2$. The nodes are approximated by $z_n^{(1)}(j) = d_j e^{-c_j n}$ and $z_j^{(1)}(n) = d_n e^{-c_n j}$, with the constants d_j, c_j and d_n, c_n also shown.

$$10 \leq x_{\text{H}} < \infty$$

	$j = 0$			$j = 1$			$j = 2$		
	$\mu(\infty)$	D	T/T_S	$\mu(\infty)$	D	T/T_S	$\mu(\infty)$	D	T/T_S
δ	1.006	1.009	2.017	1.008	1.016	2.024	1.008	1.018	2.025
b	2.553	5.302	5.439	0.071	0.148	0.157	0.002	0.003	0.004
α	2.795	2.804	2.795	2.807	2.804	2.808	2.808	2.697	2.810

Table 7

The constants δ , b , α of the least square fits for $\Delta\mu_n = \mu_\infty(\infty) - \mu_n(\infty) = \frac{b_\mu}{(x_{\text{H}})^{\delta_\mu}} e^{-\alpha_\mu n}$ (and analogous for D and T/T_S) for the SO(3) EYMD sequences $(0, n)$, $(1, 1 + n)$ and $(2, 2 + n)$ for $\gamma = 1$ and $x_{\text{H}} \geq 10$. For $x_{\text{H}} \leq 1$ see [37].

Matter Function ($x_H=0.01$)

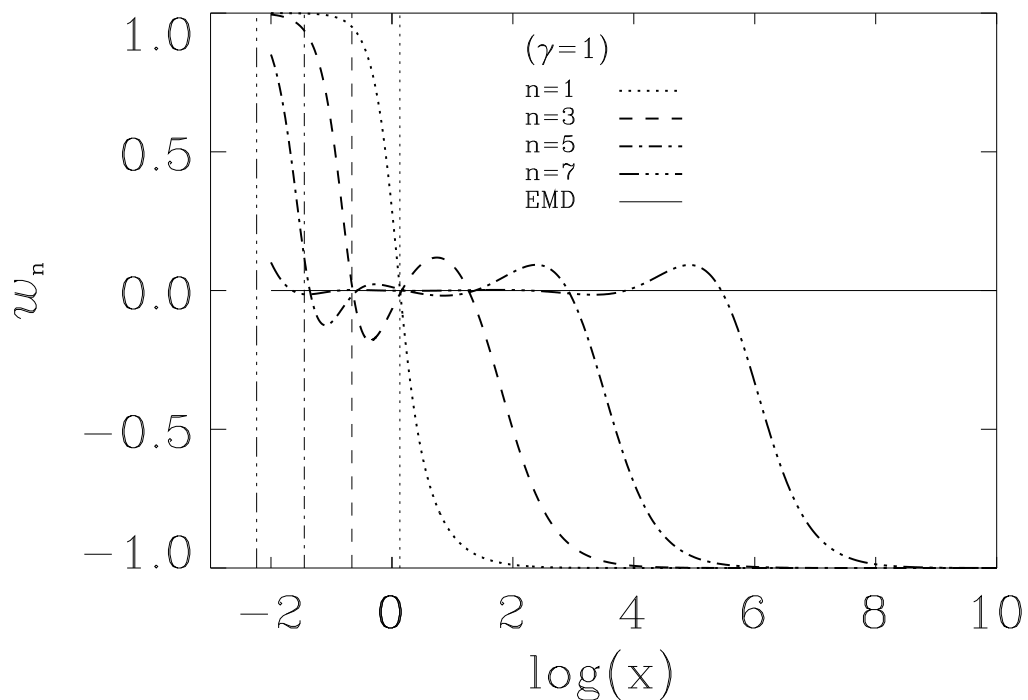


Figure 1a: The SU(2) EYMD gauge field functions $w_n(x)$ with node number $n = 1$ (dotted), $n = 3$ (dashed), $n = 5$ (dot-dashed) and $n = 7$ (triple-dot-dashed) for the black hole solutions with horizon $x_H = 0.01$ and dilaton coupling constant $\gamma = 1$. The solid line shows the gauge field function of the limiting EMD solution with the same horizon and dilaton coupling constant. The thin vertical lines indicate the location of the innermost node of the corresponding regular solutions.

Dilaton Function ($x_H=0.01$)

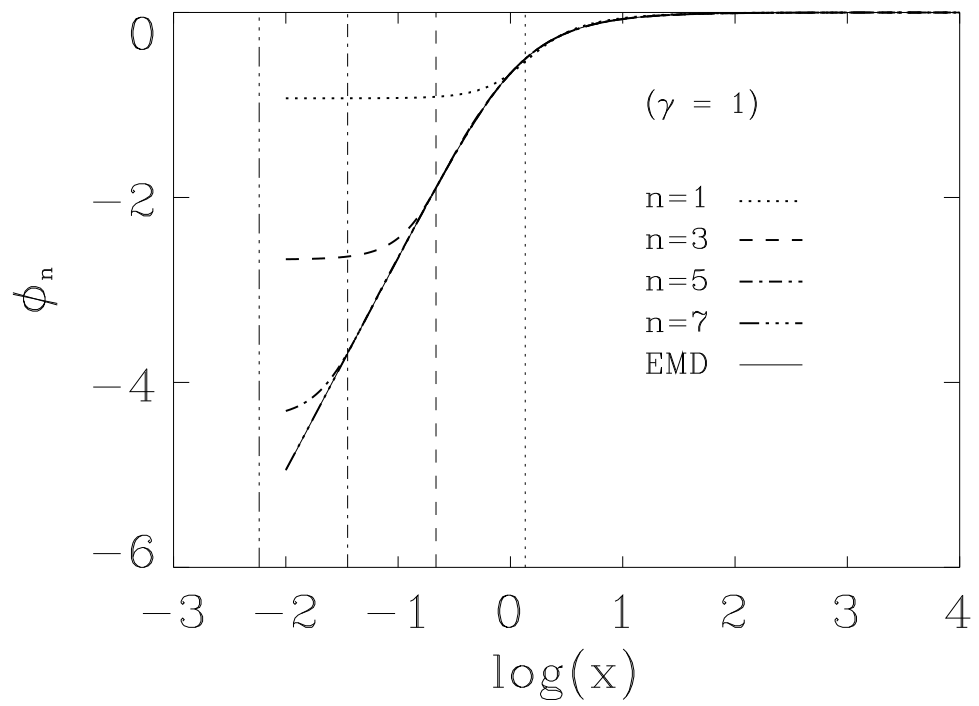


Figure 1b: Same as Figure 1a for the dilaton functions $\phi_n(x)$.

Metric Function ($x_H=0.01$)

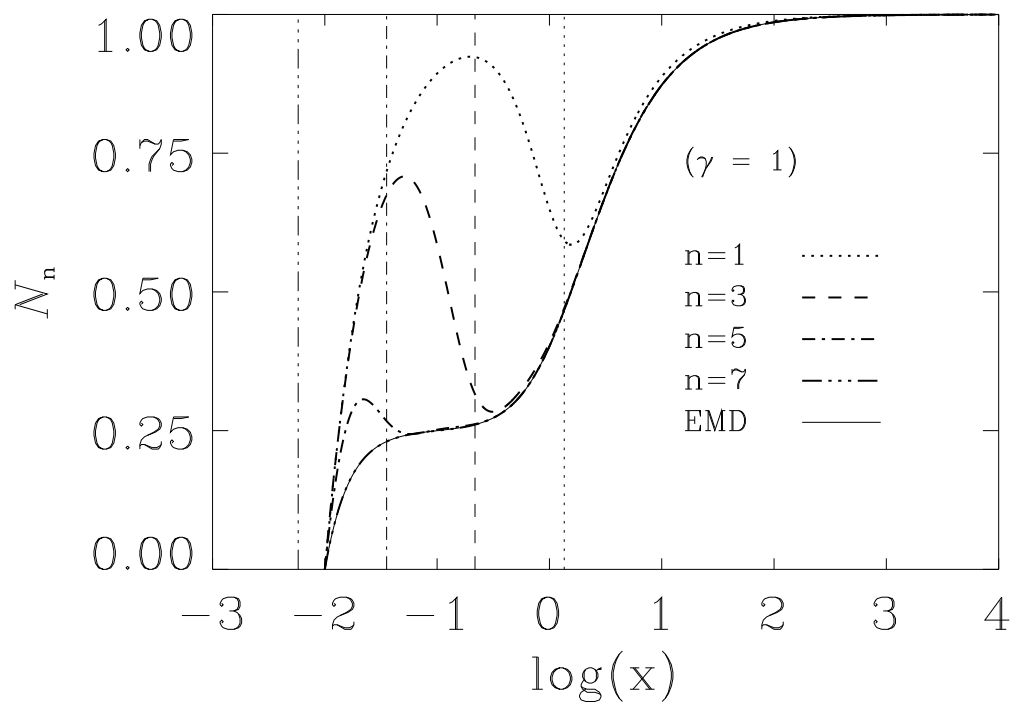


Figure 1c: Same as Figure 1a for the metric functions $N_n(x)$.

Metric Function ($x_H=0.01$)

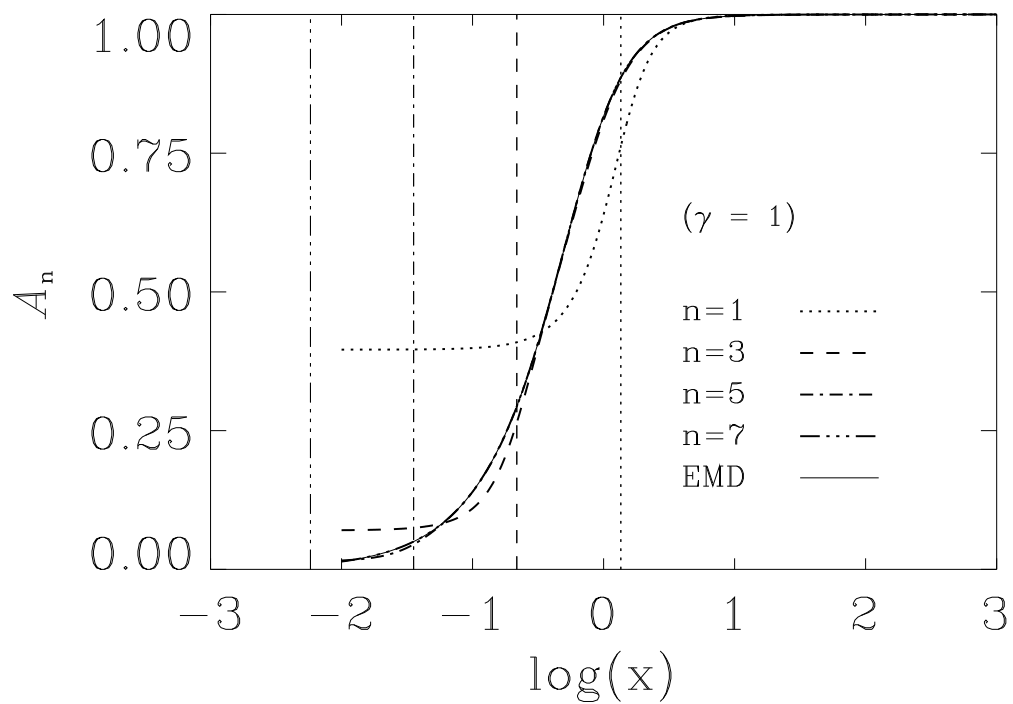


Figure 1d: Same as Figure 1a for the metric functions $A_n(x)$.

Charge ($x_H=0.01$)

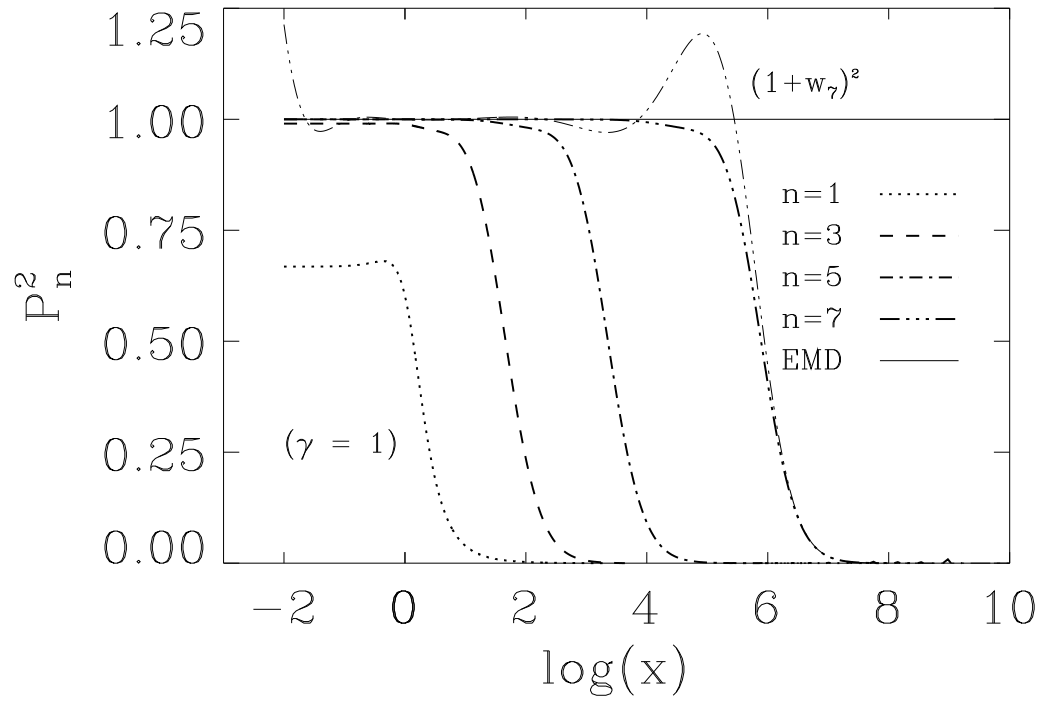


Figure 1e: Same as Figure 1a for the squared charge functions $P_n^2(x)$. Also the function $(1 + w_7(x))^2$ is shown (thin tripledot-dashed).

Matter Function (reg.)

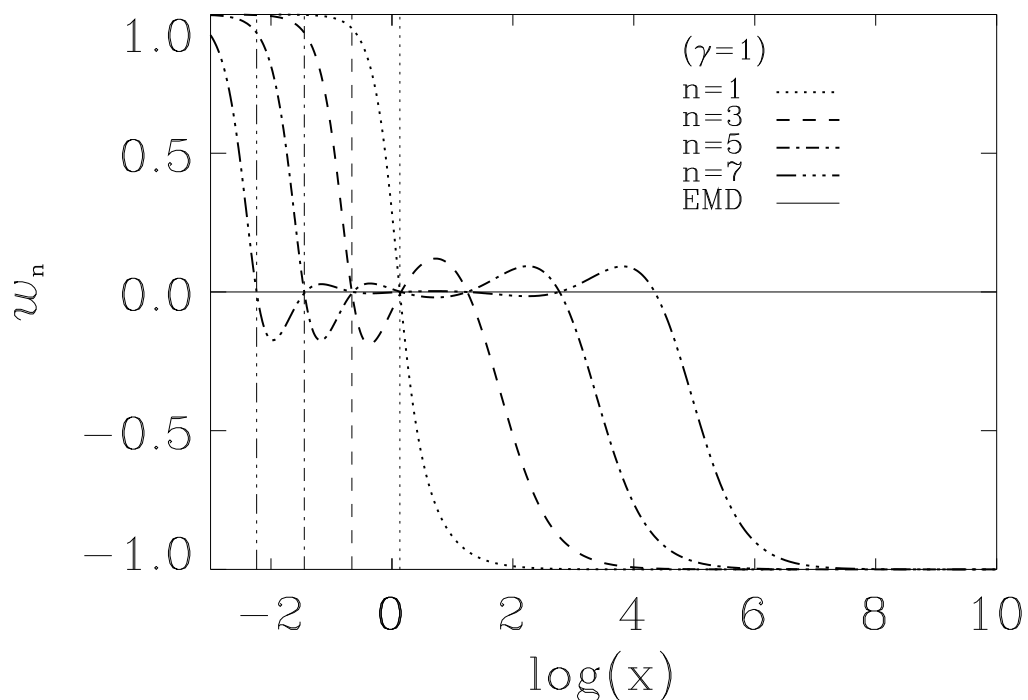


Figure 2a: The SU(2) EYMD gauge field functions $w_n(x)$ with node number $n = 1$ (dotted), $n = 3$ (dashed), $n = 5$ (dot-dashed) and $n = 7$ (triple-dot-dashed) for the regular solutions with dilaton coupling constant $\gamma = 1$. The solid line shows the gauge field function of the “extremal” EMD solution with the same dilaton coupling constant. The thin vertical lines indicate the location of the innermost nodes.

Metric Function (reg.)

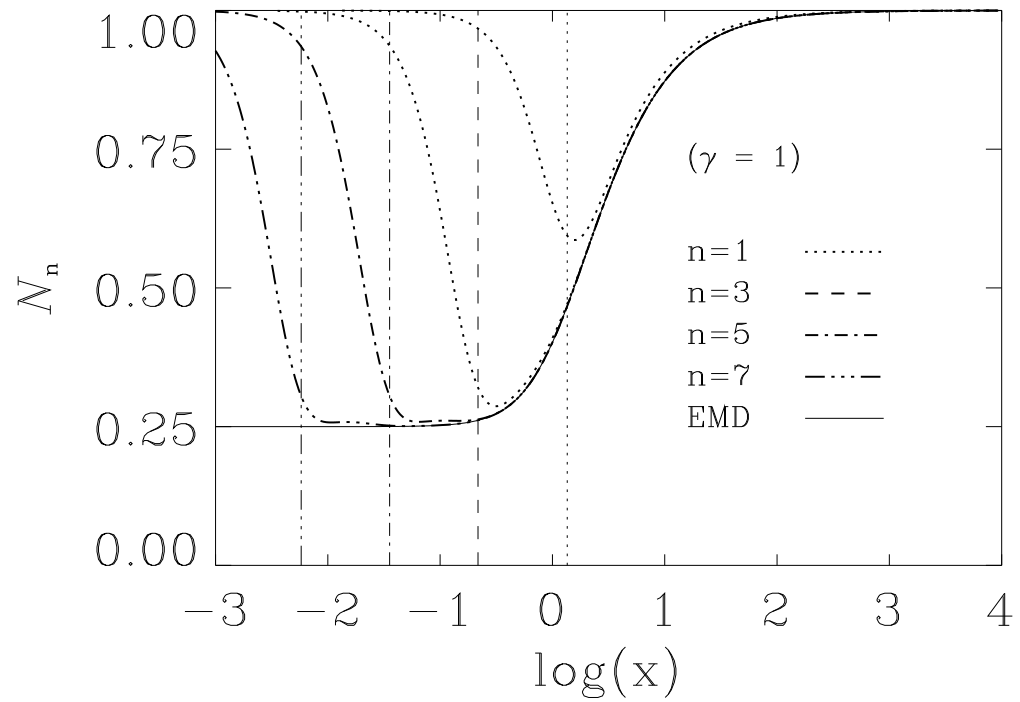


Figure 2b: The same as Figure 2a for the metric functions $N_n(x)$.

Matter Function

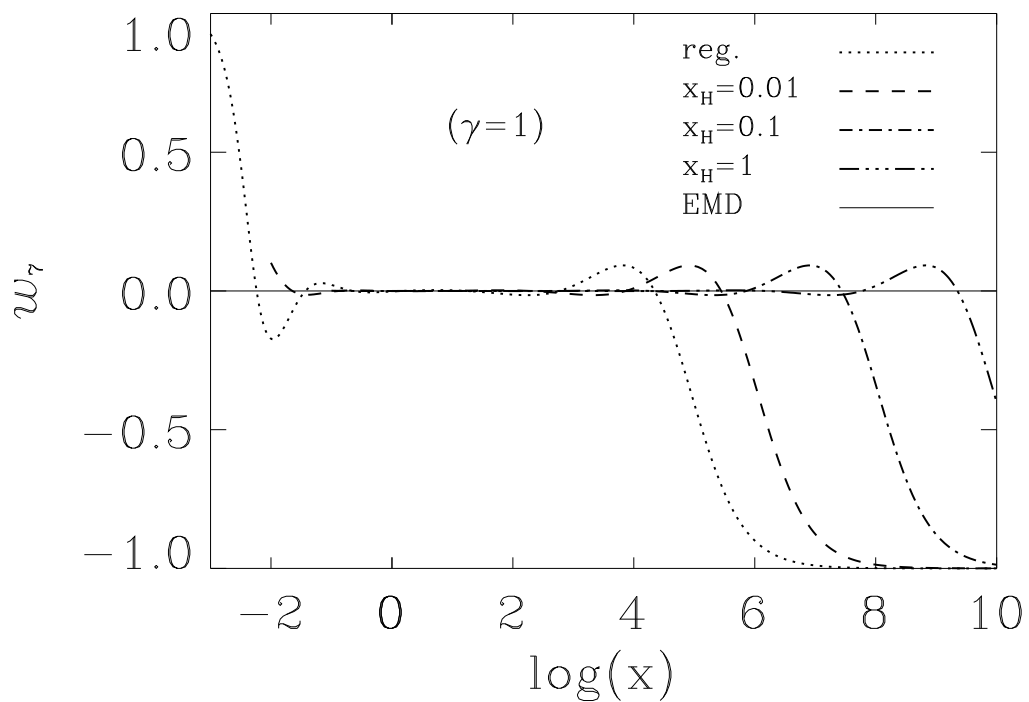


Figure 3: The SU(2) EYMD gauge field functions $w_7(x)$ for the regular solution (dotted) and the black hole solutions with horizon $x_H = 0.01$ (dashed), $x_H = 0.1$ (dot-dashed) and $x_H = 1$ (triple-dot-dashed) for the dilaton coupling constant $\gamma = 1$. The solid line shows the gauge field function of the “extremal” EMD solution.

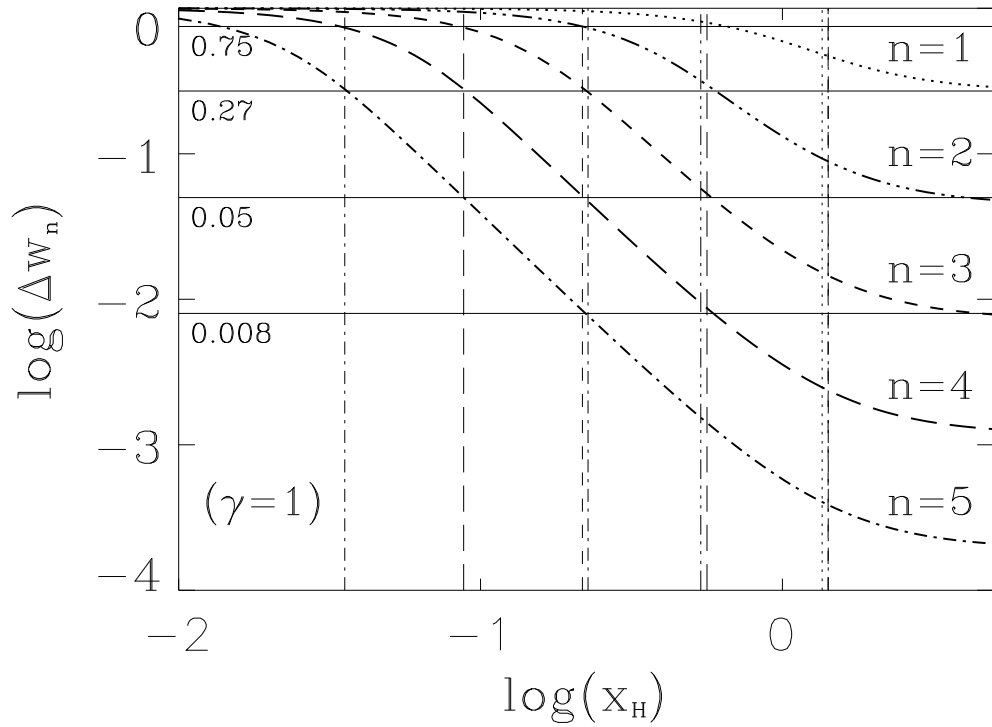


Figure 4a: The deviation at the horizon $\Delta w_n(x_H) = |w_n(x_H) - w_\infty(x_H)|$ for the SU(2) EYMD gauge field functions with up to five nodes as a function of the horizon x_H for the dilaton coupling constant $\gamma = 1$. The vertical lines indicate the location of the innermost and second nodes of the corresponding regular solutions. The horizontal lines show the deviations of 0.75, 0.27, 0.05 and 0.008 from the limiting value.

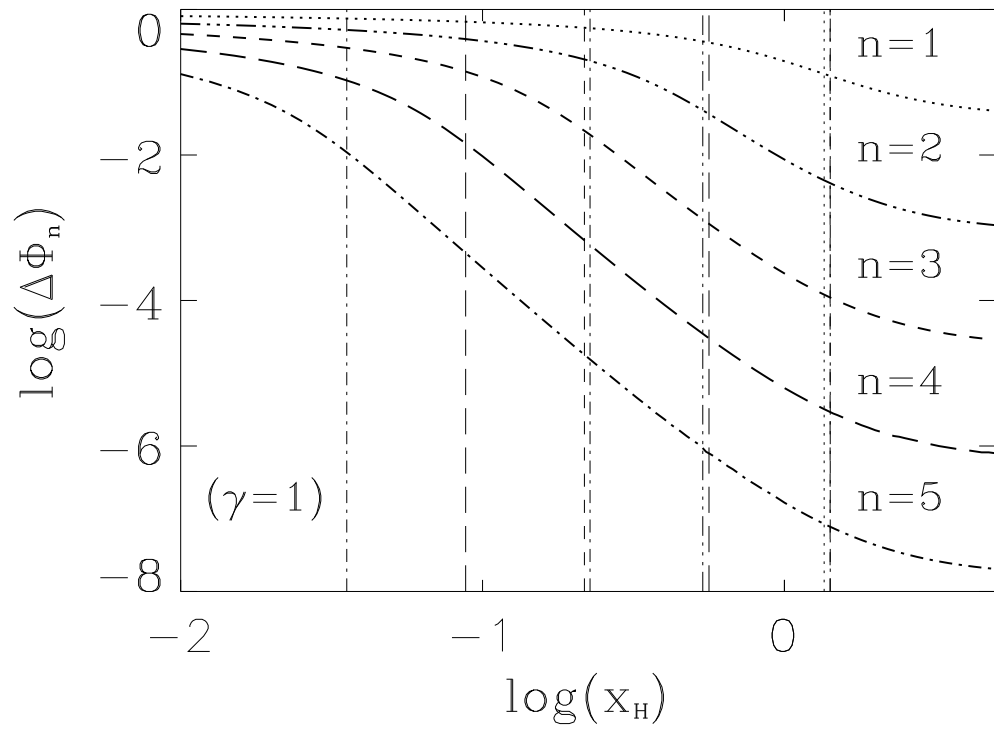


Figure 4b: The relative deviation at the horizon $\Delta\phi_n(x_H) = |(\phi_n(x_H) - \phi_\infty(x_H))/\phi_\infty(x_H)|$ for the SU(2) EYMD dilaton functions with up to five nodes as a function of the horizon x_H for the dilaton coupling constant $\gamma = 1$. The vertical lines indicate the location of the innermost and second nodes of the corresponding regular solutions.

Hawking Temperature

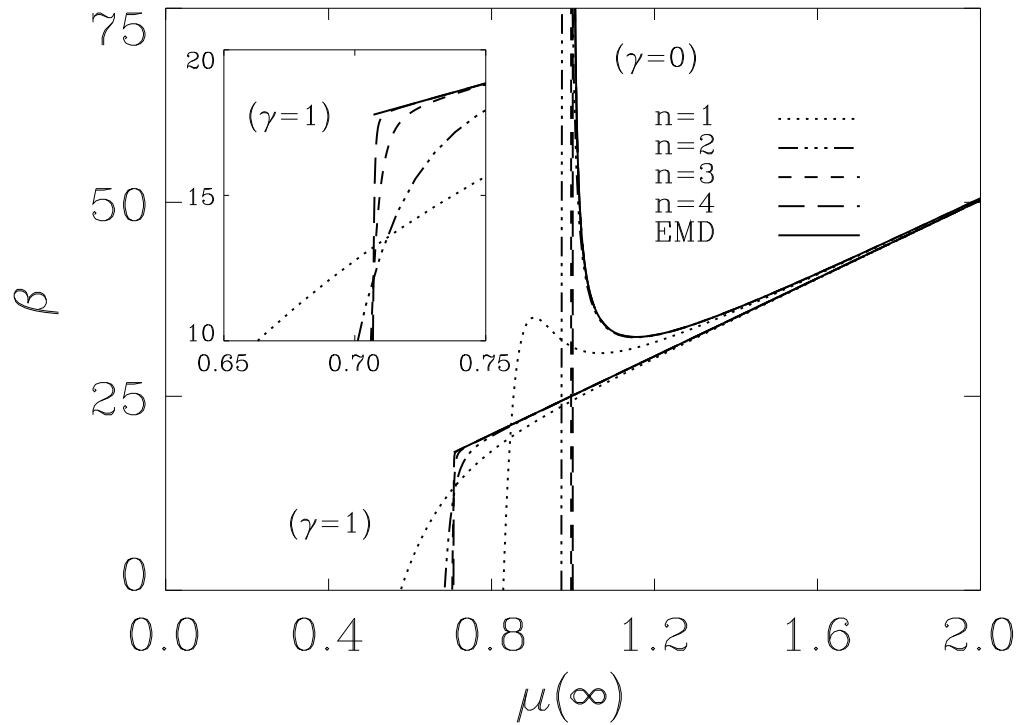


Figure 5: The inverse Hawking temperature β as a function of the mass $\mu(\infty)$ for the SU(2) EYMD solutions with node number $n = 1$ (dotted), $n = 2$ (triple-dot-dashed), $n = 3$ (dashed) and $n = 4$ (long dashed) for dilaton coupling constants $\gamma = 1$ and $\gamma = 0$. The solid lines show the inverse Hawking temperature of the EMD and RN solutions, respectively.

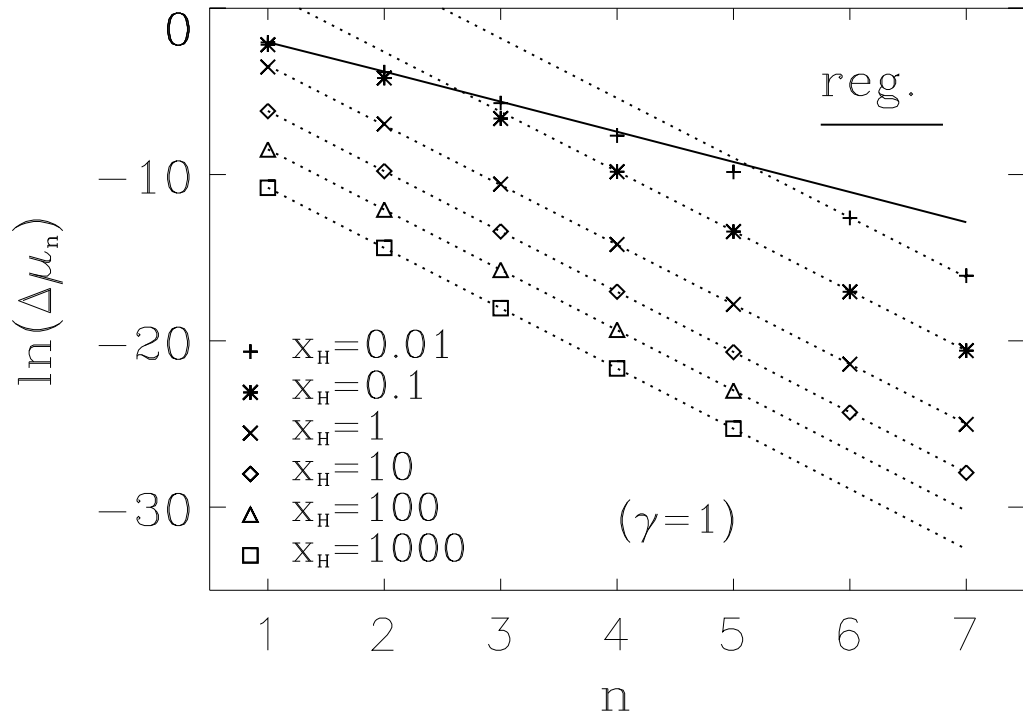


Figure 6: The logarithm of the absolute deviation from the limiting solution $\Delta\mu_n = \mu_\infty(\infty) - \mu_n(\infty)$ for the SU(2) EYMD masses as a function of the node number n with dilaton coupling constant $\gamma = 1$ for the regular solution (solid line) and the black hole solutions ($x_H = 0.01, 0.1, 1, 10, 100$ and 1000). The dotted lines indicate the least square fits with fit constants given in Table 3.

Matter Function ($x_H=0.01$)

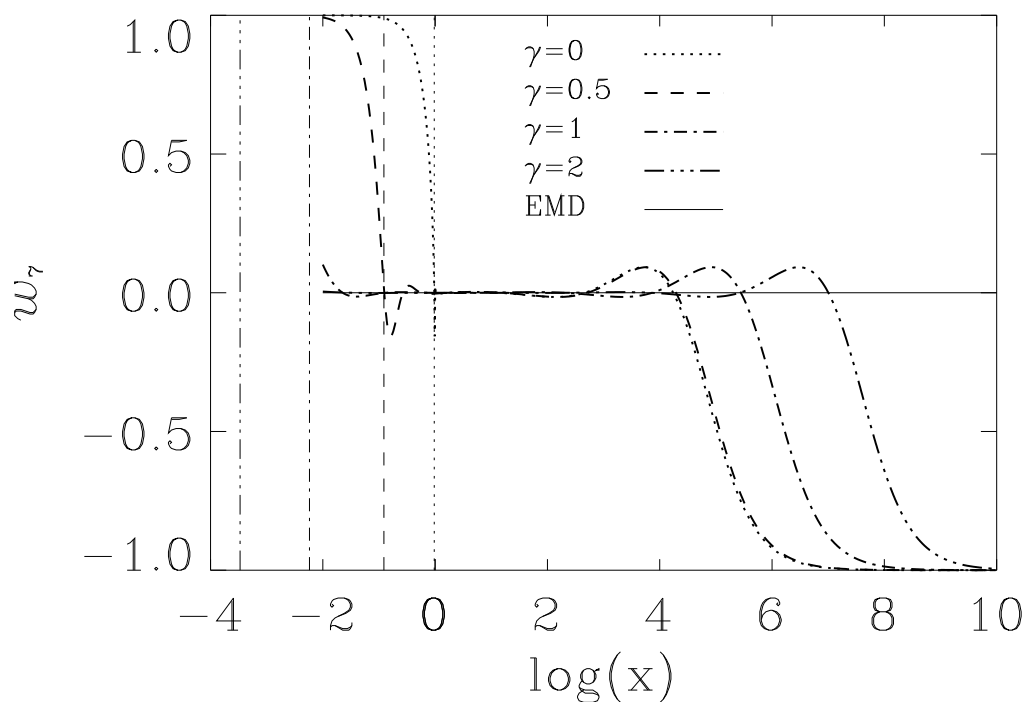


Figure 7a: The SU(2) EYMD gauge field function w_7 of the black hole solutions with horizon $x_H = 0.01$ and dilaton coupling constants $\gamma = 0$ (dotted), $\gamma = 0.5$ (dashed), $\gamma = 1$ (dot-dashed) and $\gamma = 2$ (triple-dot-dashed). The solid line shows the gauge field function of the EMD solution. The thin vertical lines indicate the location of the innermost node of the corresponding regular solutions.

Metric Function ($x_H=0.01$)

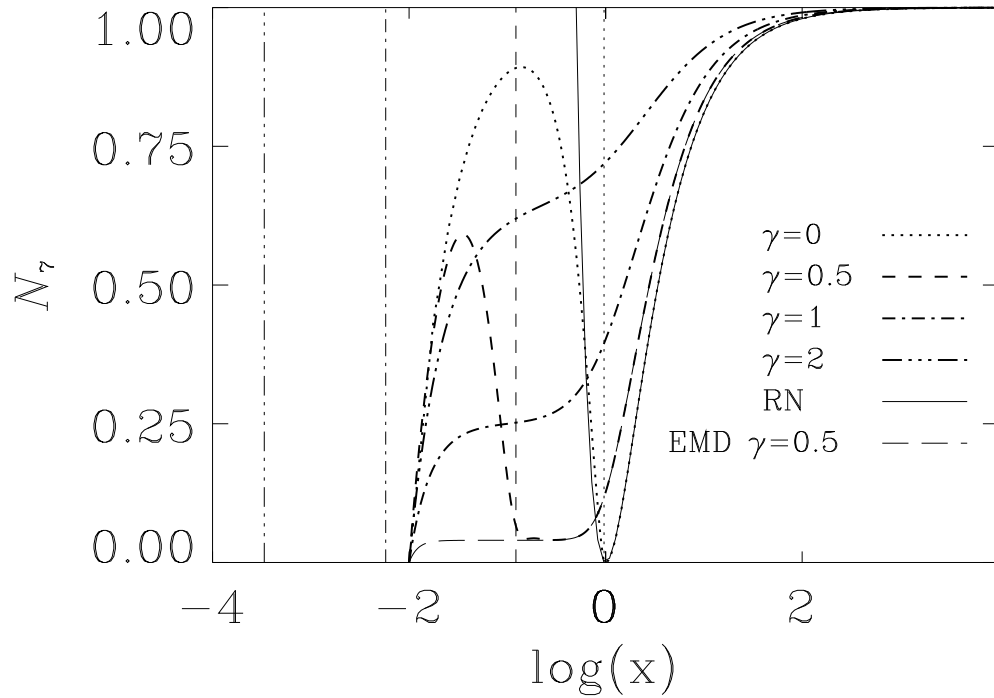


Figure 7b: The SU(2) EYMD metric functions $N_\gamma(x)$ of the black hole solutions with horizon $x_H = 0.01$ and dilaton coupling constants $\gamma = 0$ (dotted), $\gamma = 0.5$ (dashed), $\gamma = 1$ (dot-dashed) and $\gamma = 2$ (triple-dot-dashed). The solid line shows the metric function of the Reissner-Nordström solution and the long dashed line the metric function of the EMD solution with $\gamma = 0.5$. For $\gamma = 1$ and 2 the functions $N_\gamma(x)$ and their limiting EMD functions fall on top of each other and are indistinguishable. The thin vertical lines indicate the location of the innermost node of the corresponding regular solutions.

Hawking Temperature

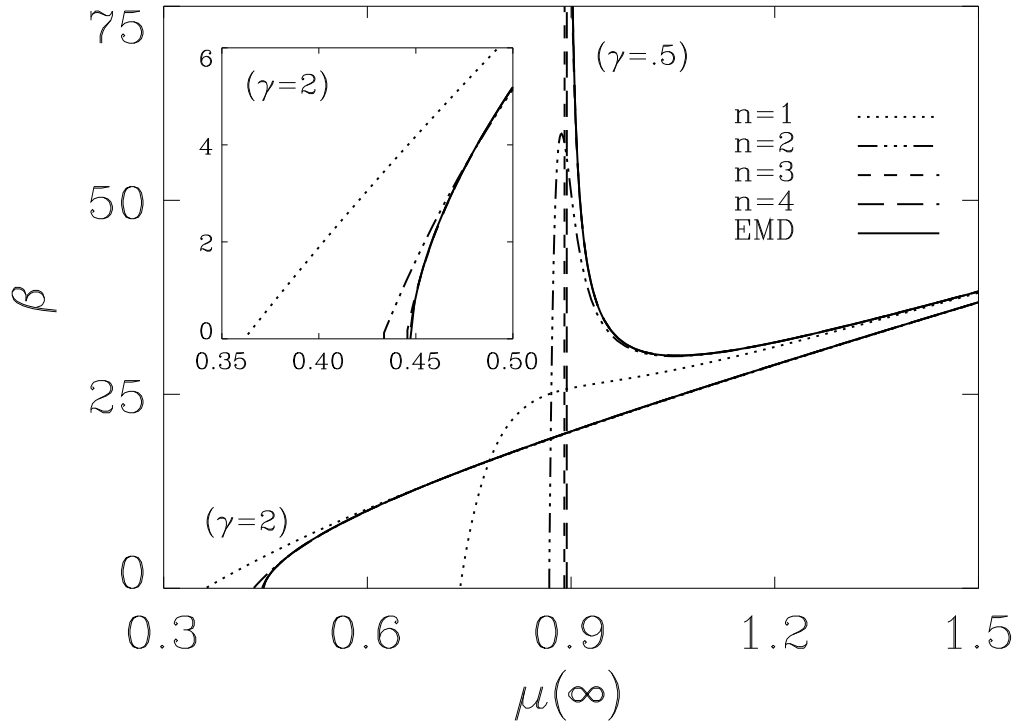


Figure 8: The inverse Hawking temperature β as a function of the mass $\mu(\infty)$ for the SU(2) EYMD solutions with node number $n = 1$ (dotted), $n = 2$ (triple-dot-dashed), $n = 3$ (dashed) and $n = 4$ (long dashed) for the dilaton coupling constants $\gamma = 0.5$ and $\gamma = 2$. The solid lines show the inverse Hawking temperature of the corresponding limiting EMD solutions.

Matter Function (5,5)

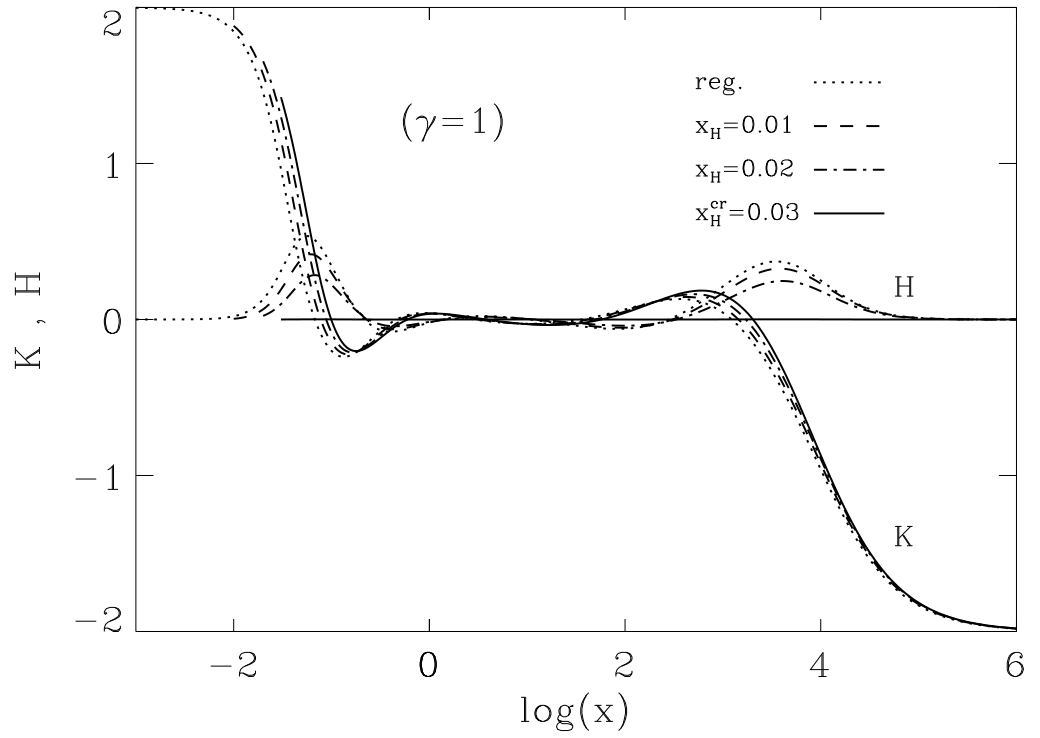


Figure 9: The SO(3) EYMD gauge field functions $K_5(x)$ and $H_5(x)$ for the regular solution (dotted) and black hole solutions with horizon $x_H = 0.01$ (dashed), $x_H = 0.02$ (dot-dashed) and $x_H^{cr} = 0.03$ (solid) with node structure (5,5) and dilaton coupling constant $\gamma = 1$.

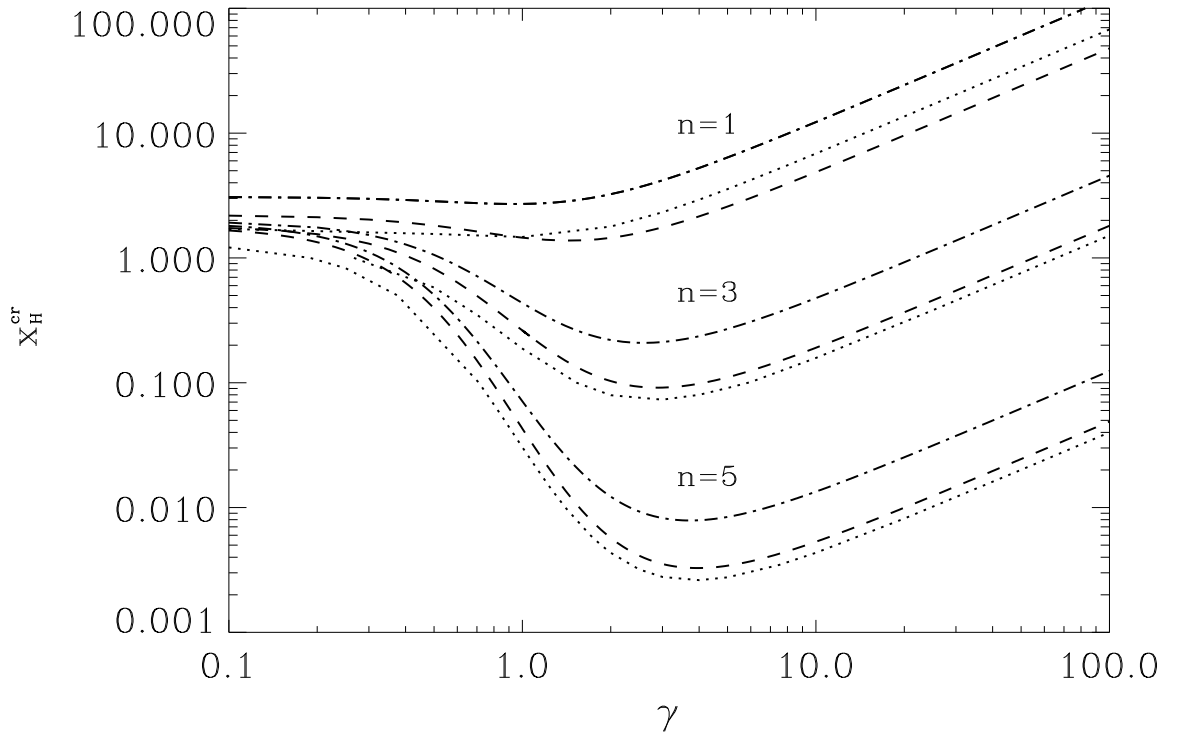


Figure 10: The critical horizon $x_H^{\text{cr}}(\gamma)$ as a function of the dilaton coupling constant γ of the SO(3) EYMD solutions with node structure (n, n) (dotted) together with the location of the innermost nodes of the corresponding regular solutions (dashed). Also shown are the locations of the innermost nodes of the scaled SU(2) solutions (dot-dashed) with the same node structure.

Matter Function ($x_H=0.2$)

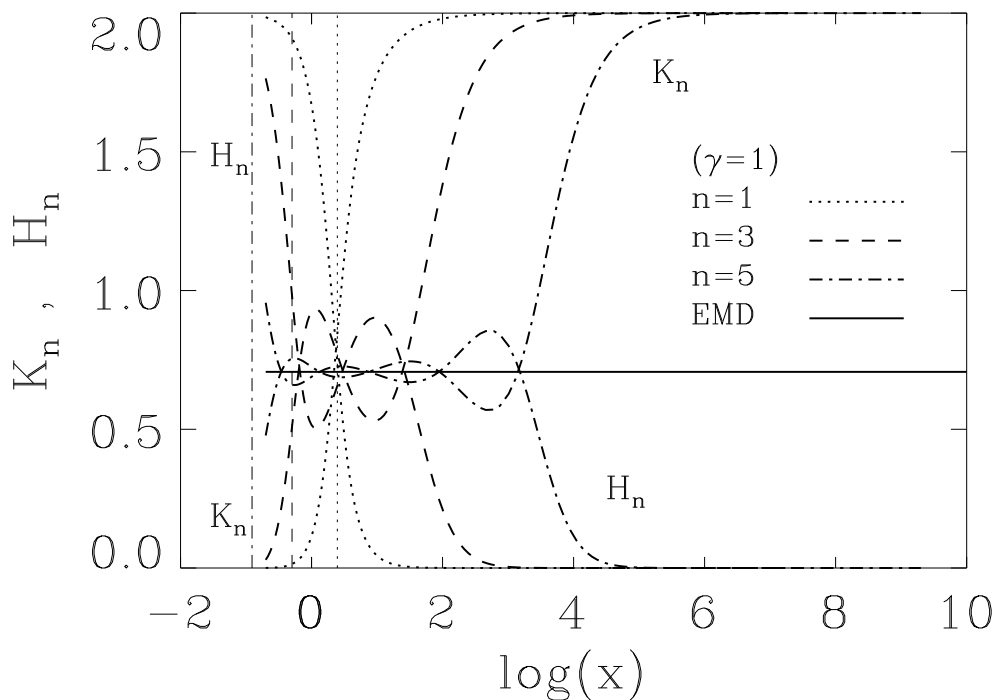


Figure 11a: The SO(3) EYMD gauge field functions $K_n(x)$ and $H_n(x)$ of the solutions with node structure $(0, n)$ for dilaton coupling constant $\gamma = 1$ and horizon $x_H = 0.2$, for $n = 1$ (dotted), $n = 3$ (dashed) and $n = 5$ (dot-dashed). The solid line shows the gauge field function of the limiting EMD solution with magnetic charge $P^2 = 3$ and the same dilaton coupling constant and horizon. The thin vertical lines indicate the location of the innermost node of the corresponding regular solutions.

Metric Function ($x_H=0.2$)

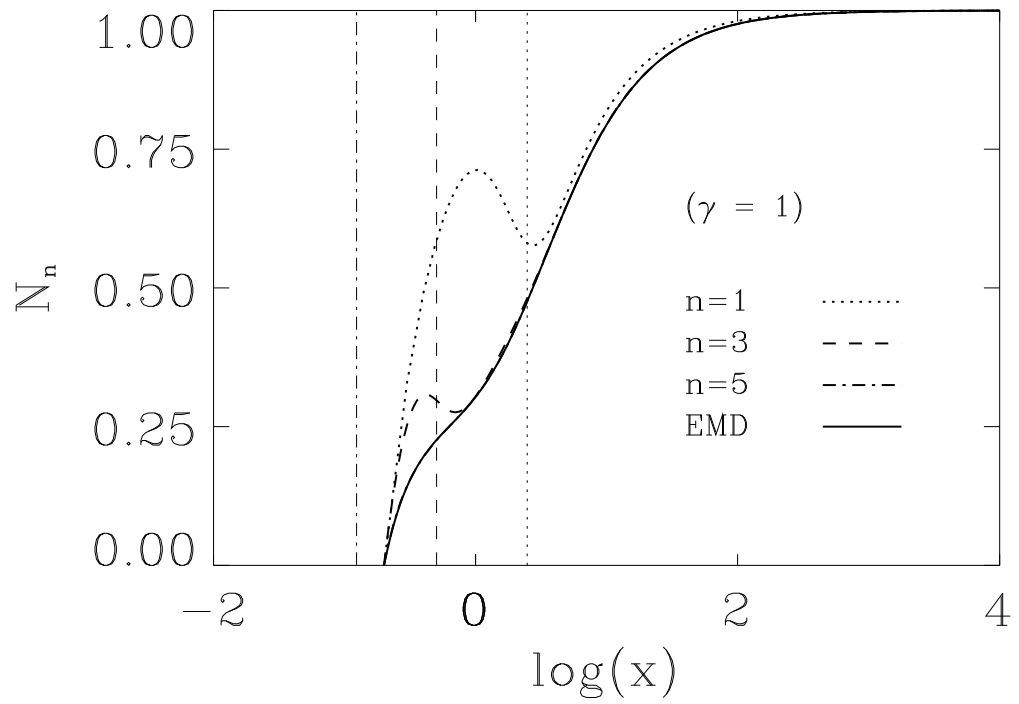


Figure 11b: The same as Figure 11a for the metric functions $N_n(x)$.

Charge ($x_H=0.2$)

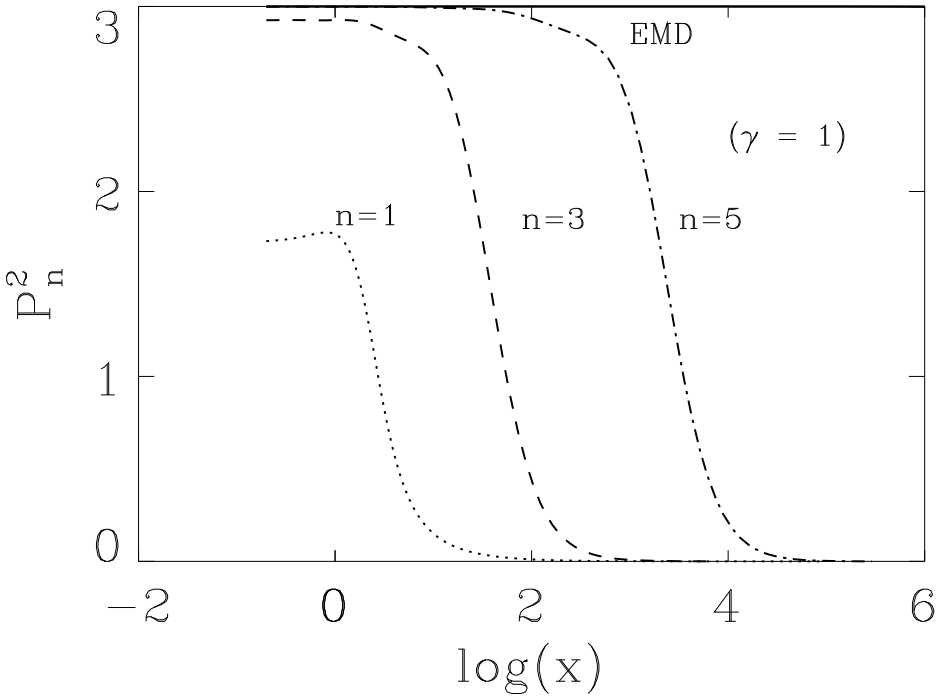


Figure 11c: The same as Figure 11a for the squared charge functions $P_n^2(x)$.

Matter Function

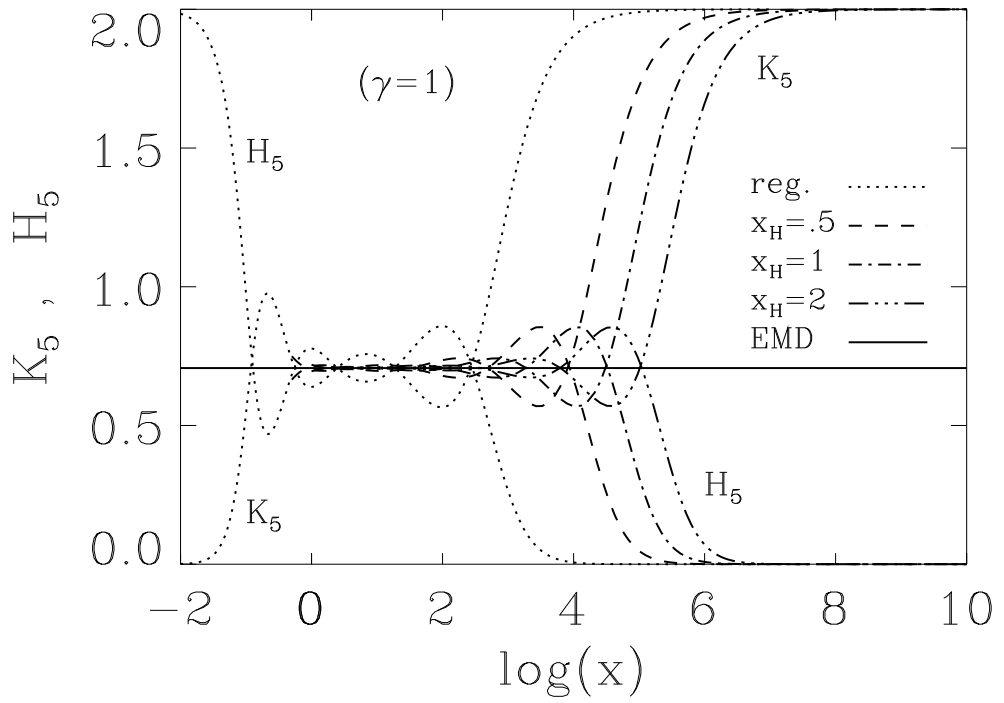


Figure 12: The SO(3) EYMD gauge field functions $K_5(x)$ and $H_5(x)$ with node structure (0, 5) and dilaton coupling constant $\gamma = 1$ for the regular solution (dotted) and black hole solutions $x_H = .5$ (dashed), $x_H = 1$ (dot-dashed) and $x_H = 2$ (triple-dot-dashed). The solid line shows the gauge field function of the “extremal” EMD solution with magnetic charge $P^2 = 3$ and the same dilaton coupling constant.

Hawking Temperature (0,n)

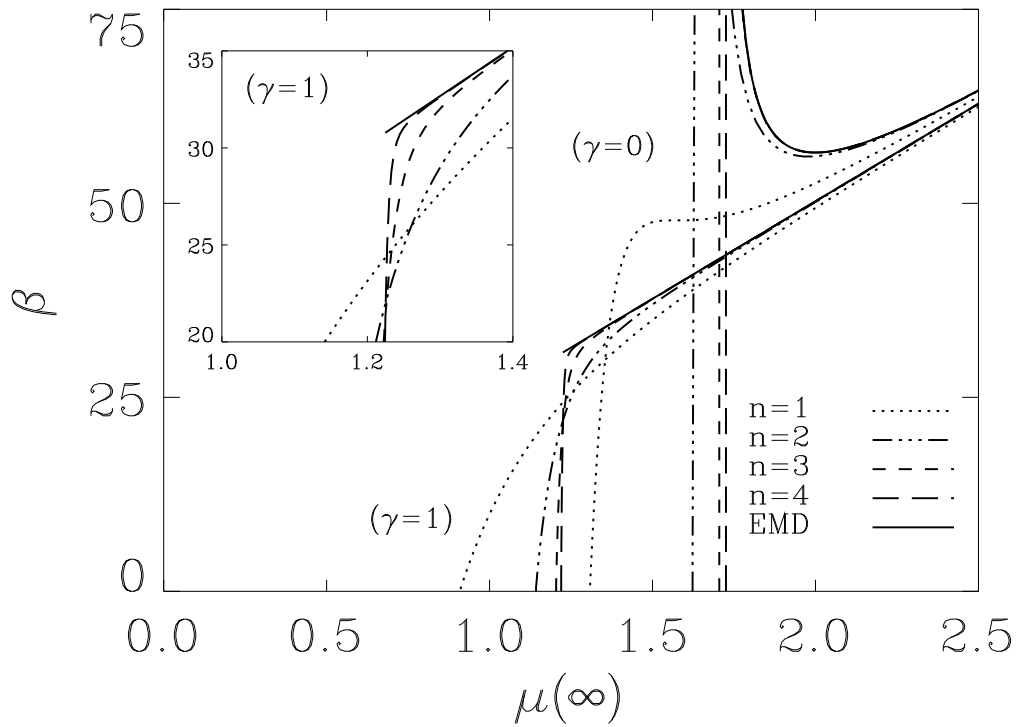


Figure 13: The inverse Hawking temperature β as a function of the mass $\mu(\infty)$ for the SO(3) EYMD solutions with node structure $(0, n)$ for the dilaton coupling constants $\gamma = 0$ and $\gamma = 1$ and node number $n = 1$ (dotted), $n = 2$ (triple-dot-dashed), $n = 3$ (dashed) and $n = 4$ (long dashed). Also shown is the inverse Hawking temperature of the limiting EMD and RN solutions (solid).

Matter Function ($x_H=0.2$)

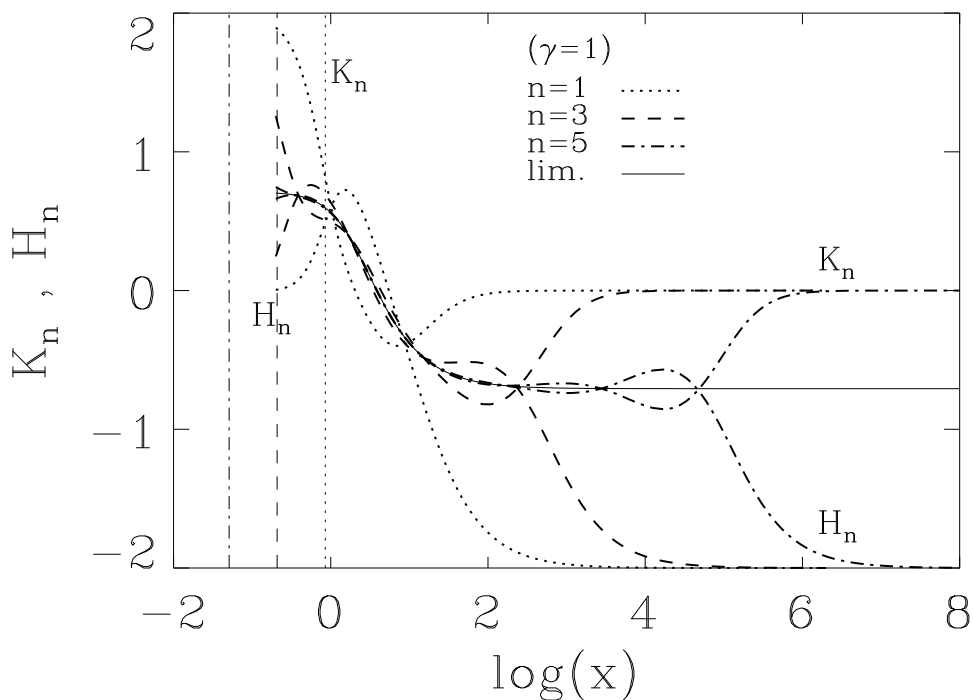


Figure 14a: The SO(3) EYMD gauge field functions $K_n(x)$ and $H_n(x)$ of the solutions with node structure $(1, 1+n)$ for the dilaton coupling constant $\gamma = 1$ and horizon $x_H = 0.2$, for $n = 1$ (dotted), $n = 3$ (dashed) and $n = 5$ (dot-dashed). The solid line shows the gauge field function of the limiting charged SU(3) EYMD solution with one node, $j = 1$, and magnetic charge $P^2 = 3$. The thin vertical lines indicate the location of the innermost node of the corresponding regular solutions.

Metric Function ($x_H=0.2$)

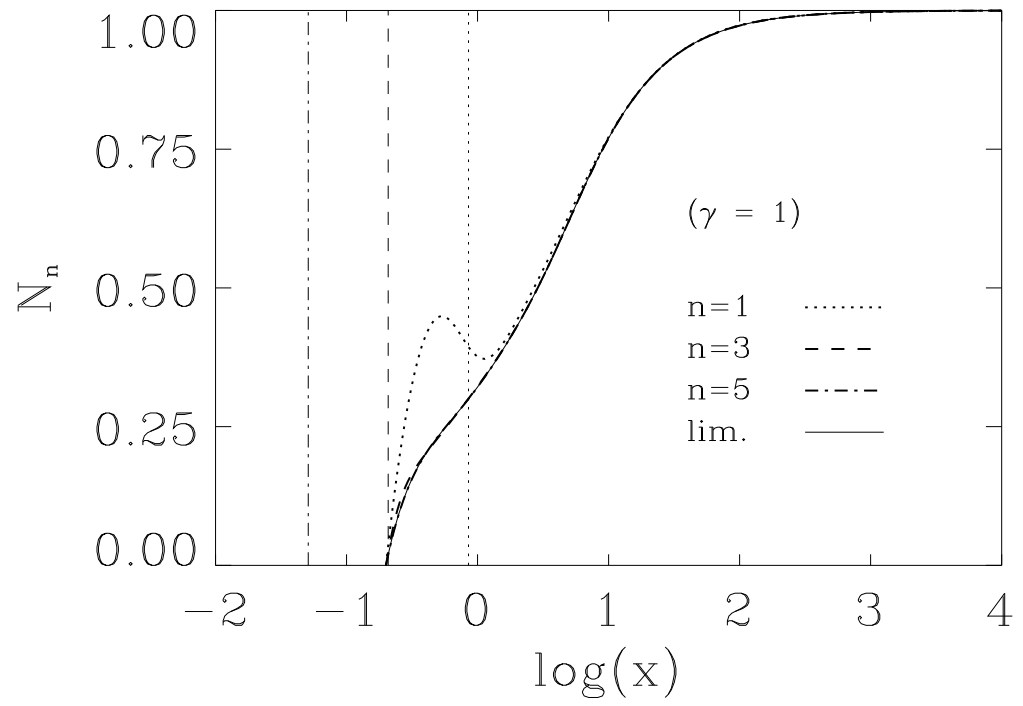


Figure 14b: The same as Figure 14a for the metric functions $N_n(x)$.

Charge ($x_H=0.2$)

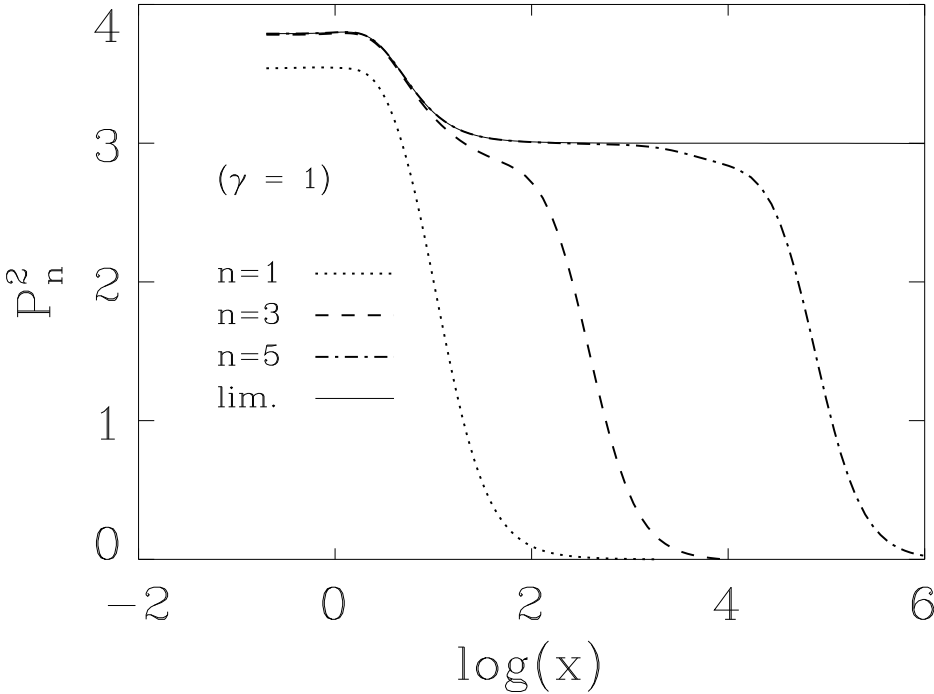


Figure 14c: The same as Figure 14a for the squared charge functions $P_n^2(x)$.

Hawking Temperature (1,1+n)

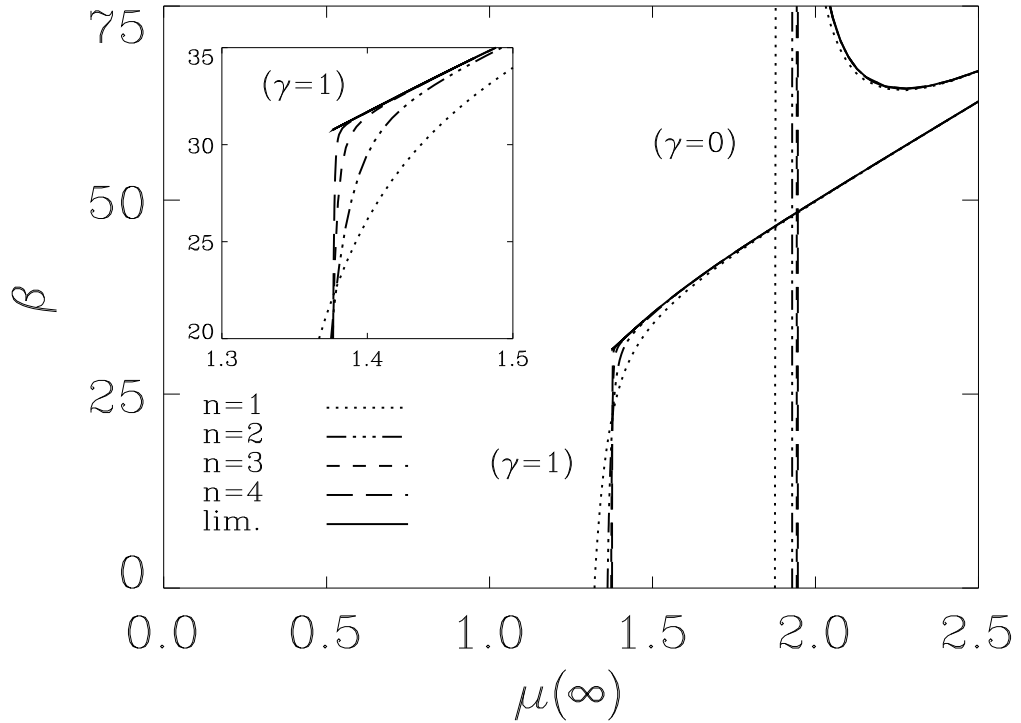


Figure 15: The inverse Hawking temperature β as a function of the mass $\mu(\infty)$ for the SO(3) EYMD solutions with node structure (1, 1+n) for the dilaton coupling constants $\gamma = 0$ and $\gamma = 1$ and node number $n = 1$ (dotted), $n = 2$ (tripledot-dashed), $n = 3$ (dashed) and $n = 4$ (long dashed). Also shown is the inverse Hawking temperature of the limiting charged SU(3) EYMD and EYM solutions with one node, $j = 1$ and magnetic charge $P^2 = 3$.

Matter Function ($x_H=0.2$)

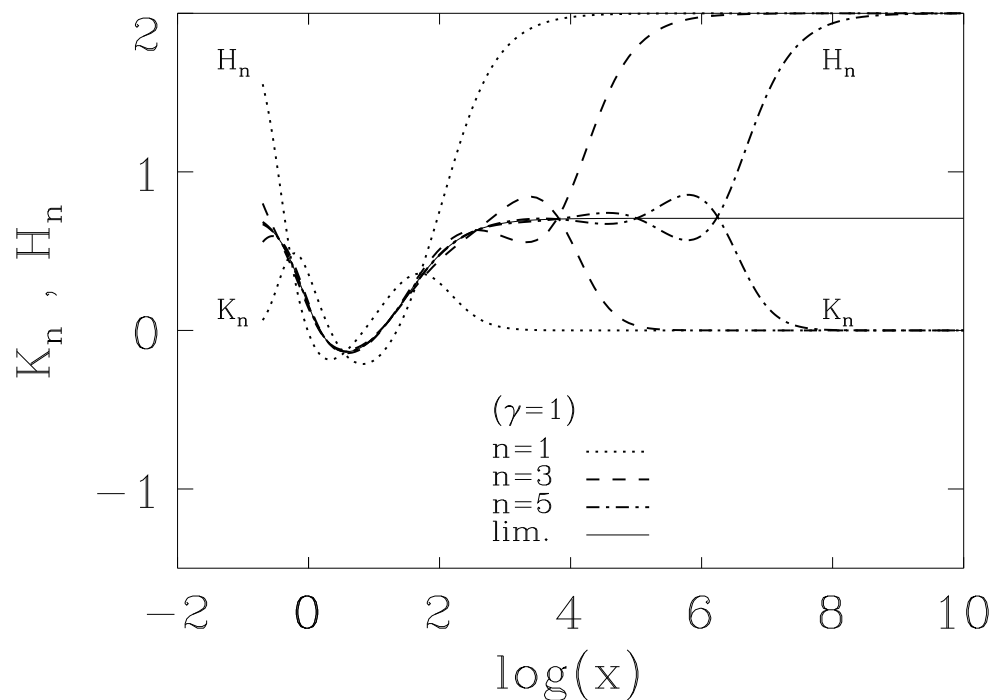


Figure 16a: The SO(3) EYMD gauge field functions $K_n(x)$ and $H_n(x)$ of the solutions with node structure $(2, 2+n)$ for the dilaton coupling constant $\gamma = 1$ and horizon $x_H = 0.2$, for $n = 1$ (dotted), $n = 3$ (dashed) and $n = 5$ (dot-dashed). The solid line shows the gauge field function of the limiting charged SU(3) EYMD solution with two nodes, $j = 2$, and magnetic charge $P^2 = 3$.

Charge ($x_H=0.2$)

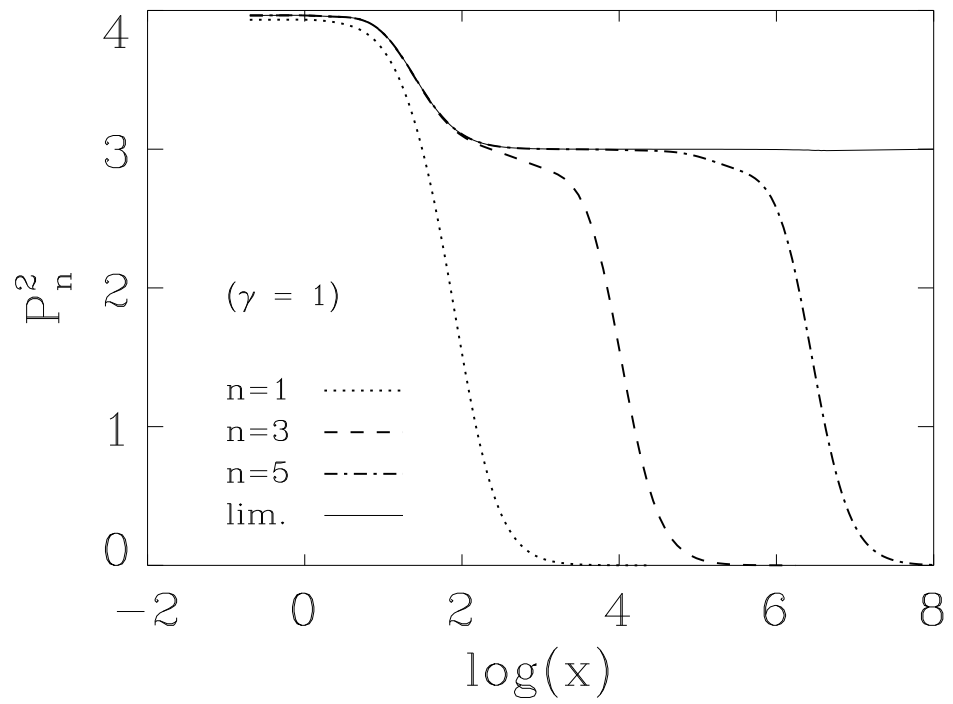


Figure 16b: The same as Figure 16a for the squared charge functions $P_n^2(x)$.

Hawking Temperature

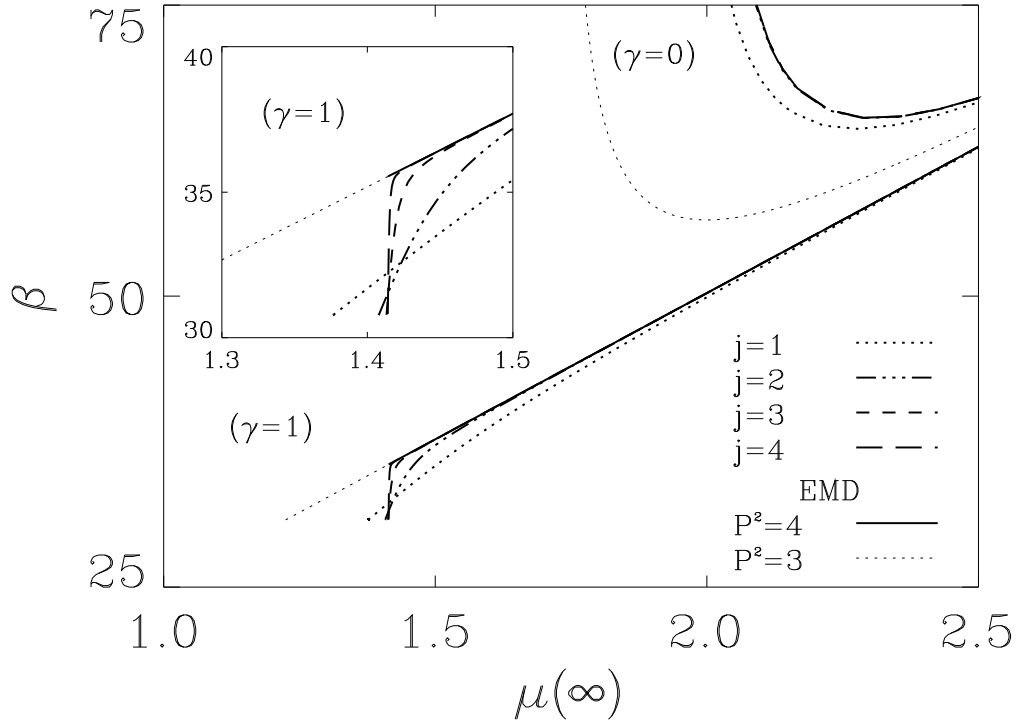


Figure 17: The inverse Hawking temperature β as a function of the mass $\mu(\infty)$ for the charged SO(3) EYM and EYMD solutions with magnetic charge $P^2 = 3$ for dilaton coupling constants $\gamma = 0$ and $\gamma = 1$ and node number $j = 1$ (dotted), $j = 2$ (triple-dotted), $j = 3$ (dashed) and $j = 4$ (long dashed). Also shown is the inverse Hawking temperature of the RN and EMD solutions with magnetic charge $P^2 = 4$ (solid) and $P^2 = 3$ (thin dotted).